

– 1 –

Gravitational Stirring in Planetary Debris Disks

Scott J. Kenyon

Smithsonian Astrophysical Observatory
60 Garden Street, Cambridge, MA 02138
e-mail: skenyon@cfa.harvard.edu

and

Benjamin C. Bromley
Department of Physics
University of Utah
201 JFB, Salt Lake City, UT 84112
e-mail:bromley@physics.utah.edu

to appear in

The Astronomical Journal
January 2001

ABSTRACT

We describe gravitational stirring models of planetary debris disks using a new multi-annulus planetesimal evolution code. The current code includes gravitational stirring and dynamical friction; future studies will include coagulation, fragmentation, Poynting-Robertson drag, and other physical processes. We use the results of our calculations to investigate the physical conditions required for small bodies in a planetesimal disk to reach the shattering velocity and begin a collisional cascade. Our results demonstrate that disks composed primarily of bodies with a single size will not undergo a collisional cascade which produces small dust grains at 30–150 AU on timescales of 1 Gyr or smaller. Disks with a size distribution of bodies reach conditions necessary for a collisional cascade in 10 Myr to 1 Gyr if the disk is at least as massive as a minimum mass solar nebula and if the disk contains objects with radii of 500 km or larger. The estimated ~ 500 Myr survival time for these disks is close to the median age of ~ 400 Myr derived for nearby stars with dusty disks.

Subject headings: planetary systems – solar system: formation – stars: formation – circumstellar matter

1. INTRODUCTION

Planetary debris disks surround nearly all stars during the early stages of their main sequence lifetimes. Recent surveys with the *Infrared Space Observatory (ISO)* indicate a median disk lifetime of $\sim 400 \times 10^6$ yr (Myr hereafter; Becklin *et al.* 1998; Dominik *et al.* 1998; Gaidos 1999; Habing *et al.* 1999; Fajardo-Acosta *et al.* 1999; Song *et al.* 2000). The disk fraction decreases dramatically with age and is much less than 10% for stars with ages of 10^9 yr (Gyr hereafter) or larger.

Because thermal emission from cold dust is large compared to the photospheric radiation from the central star, most debris disks have been detected with mid-infrared or far-infrared observations (Backman & Paresce 1993; Artymowicz 1997; Lagrange *et al.* 2000). Infrared and optical images reveal a disk-like morphology with an outer radius ranging from 100–200 AU up to 1000 AU in several systems (Augereau *et al.* 1999a, 1999b; Greaves *et al.* 1998; Holland *et al.* 1998; Jayawardhana *et al.* 1998, 2000; Koerner *et al.* 1998; Schneider *et al.* 1999; Trilling & Brown 1998; Trilling *et al.* 2000). The disk often has a central ‘hole,’ where radiation from small dust grains is less than emission from material in the outer disk. The ratio of disk to stellar luminosity is $L_d/L_\star \sim 10^{-5}$ to 10^{-2} (Artymowicz 1997; Fajardo-Acosta, Stencel, & Backman 1997; Fajardo-Acosta *et al.* 1999;

Lagrange *et al.* 2000). The disks have a small gas content, with measured gas-to-dust mass ratios of $M_g/M_d \lesssim 1\text{--}10$ (Zuckerman *et al.* 1995; Dent *et al.* 1995; Lecavelier des Etangs, Vidal-Madjar, & Ferlet 1998; Greaves, Coulson, & Holland 2000). Models for the scattered and thermal emission suggest grains with sizes of 1–100 μm and a total mass in small grains of $\sim 0.01 M_E$, where $1 M_E = 6 \times 10^{27} \text{ g}$ is the mass of the earth (e.g., Greaves, Mannings, & Holland 2000).

Theoretical models for a debris disk begin with dust grains in Keplerian orbits about the central star (see Artymowicz 1997, Lagrange *et al.* 2000, and references therein). For particle sizes of 1–100 μm , Poynting-Robertson drag and radiation pressure remove dust from the disk in $\sim 1\text{--}10 \text{ Myr}$ (Burns *et al.* 1979; Backman & Paresce 1993; Backman, Dasgupta, & Stencel 1995; Artymowicz 1997). Collisions between larger bodies can replenish small grains if the collision velocity is $\sim 100\text{--}300 \text{ m s}^{-1}$ (see below). These large velocities initiate a “collisional cascade,” where planetesimals with radii of 1–10 km are ground down into smaller and smaller bodies. A collisional cascade requires a mass reservoir of $\sim 10\text{--}100 M_E$ to replenish smaller grains over a disk lifetime of 100 Myr or more (Artymowicz 1997; Habing *et al.* 1999). This mass is similar to estimates for the original planetesimal mass in the Kuiper Belt of our Solar System (e.g., Stern 1995, 1996; Kenyon & Luu 1998 [KL98], 1999 [KL99]).

Despite the popularity of this picture, the origin of the large collision velocities is uncertain. Because the difference between the gas velocity and dust velocity is small and circularization is efficient, dust grains and larger bodies within a protosolar nebula probably had nearly circular orbits initially (see KL99 and references therein). Short-term encounters with passing stars and stirring by planets embedded in the disk can increase the velocities of dust grains (e.g., Artymowicz *et al.* 1989; Mouillet *et al.* 1997; Ida *et al.* 2000; Kalas *et al.* 2000). Although stellar encounters can increase particle velocities enormously, such encounters are probably rare. Collisions of bodies within the disk may also effectively damp large velocities following the encounter; KL99 estimate damping times of 1–10 Myr for 1–100 m objects during the early stages of planetesimal growth in the Kuiper Belt. Stirring by embedded planets is attractive, because objects with radii of 1000 km or more naturally form in the disk and these objects continuously stir up the velocities of small dust grains.

The timescale to reach the large collision velocities required in many debris disks is uncertain. Kenyon *et al.* (1999) show that Pluto-sized objects can form within the dusty ring of HR4796 A and stir up the velocities of smaller objects in $\sim 10 \text{ Myr}$ if the disk is sufficiently massive. Gravitational stirring may be less efficient in lower mass disks (KL99) and in the outer portions of the debris disks of β Pic and other systems.

Our goal is to investigate the physical conditions needed in a planetary debris disk for embedded planets to stir up smaller objects to the shattering velocity. We use a new multi-annulus planetesimal evolution code to compute the dynamical evolution of small

bodies and show that results for simple test problems agree with previous calculations. Our calculations for debris disks with masses comparable to the ‘minimum mass solar nebula’ indicate that small bodies with radii of 200 km or less can stir much smaller bodies in the disk on timescales of 1 Gyr or longer. Shorter stirring timescales require larger objects and more massive disks. Objects with radii of 500 km or larger can stir low mass planetesimals to the shattering limit in disks with 5–10 times the mass of a minimum mass solar nebula in 10–20 Myr, close to the inferred ages for β Pic and HR 4796A (Barrado y Navascués *et al.* 1997, 1999; see also Song *et al.* 2000). Once small bodies reach the shattering limit, the lifetime of small bodies at 100 AU is roughly 500 Myr for a minimum mass solar nebula. These results suggest that planetesimal growth in protosolar nebulae with a range of initial masses can account for the observed range of ages of planetary debris disk systems.

We outline the model in §2, describe the calculations in §3, and conclude with a brief discussion in §4.

2. The Model

As in KL98 and KL99, we adopt Safronov’s (1969) particle-in-a-box method, where we treat planetesimals as a statistical ensemble of masses with a distribution of horizontal and vertical velocities about a Keplerian orbit¹. The model grid contains N concentric annuli centered at heliocentric distances a_i . Each annulus has an inner radius at $a_i - \delta a_i/2$ and an outer radius at $a_i + \delta a_i/2$. The midpoint of the model grid is at a heliocentric distance a_{mid} . Calculations begin with a differential mass distribution $n(m_i)$ of bodies with horizontal and vertical velocity dispersions $h_i(t)$ and $v_i(t)$. We approximate the continuous distribution of particle masses with discrete batches having particle populations $n_i(t)$ and total masses $M_i(t)$.

To evolve the velocity distribution in time, we solve the Fokker-Planck equation for an ensemble of masses undergoing dynamical friction and viscous stirring. Dynamical friction transfers kinetic energy from large bodies to small bodies and drives a system to energy equipartition. Viscous stirring converts energy from the stellar potential into random motion and increases the velocities of all planetesimals. We do not allow physical collisions in this study; all gravitational interactions are elastic and do not modify the initial mass distribution. The Appendices of KL98 and KL99 describe accretion and velocity evolution for planetesimals in a single annulus and compare numerical results with analytic solutions for standard test cases. The Appendix of this paper generalizes KL98 and KL99 for a disk with N concentric annuli and describes several test cases (see also Spaute *et al.* 1991;

¹Kokubo & Ida (1996) compare several results from this statistical theory to results of direct n -body calculations.

Weidenschilling *et al.* 1997).

The starting conditions for these calculations are based on KL99 and Kenyon *et al.* (1999). We consider systems of N annuli in disks with $a_{mid} = 35\text{--}140$ AU and $\delta a_i/a_i = 0.001\text{--}0.0125$. The central star has a mass of $3 M_\odot$, appropriate for debris disks surrounding nearby A-type stars. Timescales for other central stars and other heliocentric distances scale with stellar mass and heliocentric distance as $(a^3/M_\star)^{1/2}$. The particles begin with eccentricity e_0 and inclination $i_0 = e_0/2$. The initial velocities are then $h_{i0} = 0.79 e_0 V_{Ki}$ and $v_{i0} = 0.71 \sin i_0 V_{Ki}$ where V_{Ki} is the velocity of a circular orbit centered on annulus i . Several tests show that the timescale to reach large random velocities is fairly independent of e_0 for $e_0 \lesssim 10^{-3}$.

3. Calculations

3.1. A Simple Model for the Disk Lifetime

To assess the outcome of the stirring calculations, we identify models which can initiate a collisional cascade and produce enough debris to account for observations of currently known debris disk systems. The debris produced in a collision between two bodies of mass m_i and m_j is set by the center-of-mass collision energy,

$$Q_{c,ij} = \frac{0.25 m_i m_j V_{I,ij}^2}{(m_i + m_j)^2} \quad (1)$$

where $V_{I,ij}$ is the impact velocity. We adopt $V_{I,ij}^2 = V_{ij}^2 + V_{e,ij}^2$, where V_{ij} is the relative velocity of the colliding planetesimals and $V_{e,ij}^2 = 2G(m_i + m_j)/(r_i + r_j)$ is the mutual escape velocity (see the Appendix of KL99 and references therein). The energy needed to fragment the colliding bodies and eject a fraction, f_{ej} , of their combined mass is

$$Q_f = S \left(\frac{\alpha_V f_{ej}^{1 + 2/\alpha_V}}{f_{KE}(\alpha_V - 2)} \right) . \quad (2)$$

where S is the binding energy of the combined mass² (Davis *et al.* 1985; Davis, Ryan, & Farinella 1994). This expression assumes the ejected fragments receive a fixed fraction of the impact energy, $f_{KE}Q_{f,ij}$, and have a power law velocity distribution,

$$f(>v) \propto (v/v_c)^{-\alpha_V} . \quad (3)$$

²The binding energy, S , is composed of an intrinsic tensile strength, S_0 , and a gravitational binding energy. For objects with radii of 10 km or less, $S \approx S_0$; S is comparable to the gravitational binding energy for objects with radii of 100 km or larger.

If $Q_f = Q_{c,ij}$ and $\alpha_V = 2.25$ (e.g., Davis *et al.* 1985; KL99), the impact velocity needed to eject $f_{ej}(m_i + m_j)$ is

$$V_{I,ij} = 6 \left(\frac{f_{ej}^{17/9} S}{f_{KE}} \right)^{1/2} \left(\frac{m_i + m_j}{\sqrt{m_i m_j}} \right). \quad (4)$$

This expression reduces to

$$V_{I,ij} \approx 800 \text{ m s}^{-1} f_{ej}^{17/18}, \quad (5)$$

for a collision between two equal mass bodies with $S = 2 \times 10^6 \text{ erg g}^{-1}$ and $f_{KE} = 0.05$, typical values for small icy objects in the outer disk (see KL99 and references therein). For 1 km bodies with $m = 6.3 \times 10^{15} \text{ g}$, an impact velocity of 90 m s^{-1} ejects $\sim 10\%$ of the combined mass. An impact velocity of 400 m s^{-1} ejects $\sim 50\%$ of the combined mass.

To estimate the lifetime of a disk of mass M_d undergoing a collisional cascade, we use the coagulation equation (see KL98 and references therein):

$$\frac{dn_i}{dt} \approx \left(\frac{n_i n_j}{4H a \delta a} \right) V_{ij} (r_i + r_j)^2 \quad (6)$$

where r_i and r_j are the radii of the two bodies, $V_{ij}^2 = V_i^2 + V_j^2$ is the relative velocity, H is the vertical scale height, and δa is the width of an annulus centered at a . This expression neglects gravitational focusing. The production rate of debris is $\dot{m} \equiv dm/dt = f_{ej}(m_i + m_j)dn/dt$. The disk lifetime is then $\tau_d = M_d/\dot{m}$. We adopt a disk model with a surface density $\Sigma = \Sigma_0(a/a_0)^{-3/2}$ where $a_0 = 1 \text{ AU}$. The disk mass is $m_d = 2\pi\Sigma a \delta a$. Collisions between equal mass bodies yields $n_i n_j = m_d^2/2m_i^2$; the disk lifetime is then

$$\tau_d = \frac{H r_i \rho}{3\Sigma_0 f_{ej} V_{ij}} \left(\frac{a}{a_0} \right)^{3/2} \quad (7)$$

Substituting $H = 0.64 V_{ij}/\Omega_K$, where Ω_K is the orbital frequency yields

$$\tau_d = 500 \text{ Myr} \left(\frac{60 \text{ g cm}^{-2}}{\Sigma_0} \right) \left(\frac{r_i}{1 \text{ km}} \right) \left(\frac{\rho}{1.5 \text{ g cm}^{-3}} \right) \left(\frac{0.2}{f_{ej}} \right) \left(\frac{a}{100 \text{ AU}} \right)^3 \quad (8)$$

where ρ is the mass density of a planetesimal and $\Sigma_0 = 60 \text{ g cm}^{-2}$ is the surface density of the ‘minimum mass solar nebula’ (Hayashi 1981; Weidenschilling 1977). We adopt $r_i = 1 \text{ km}$, which is roughly the peak of the mass function for coagulation calculations in the outer disk (KL99; Kenyon *et al.* 1999). The observed disk lifetime of 300–500 Myr for most systems implies $f_{ej} \approx 0.2$ and an impact velocity of $\sim 175 \text{ m s}^{-1}$. The relative velocities of the 1 km planetesimals are then $\sim 125 \text{ m s}^{-1}$.

A disk with $V_{ij} = 100\text{--}200 \text{ m s}^{-1}$ and $f_{ej} = 0.2$ satisfies current constraints on the thermal emission and scattered light component of debris disks. For a disk with scale height H , the solid angle of the disk as seen from the central star is $\Omega/4\pi = H/2a \approx 0.01\text{--}0.02$ for $a = 100 \text{ AU}$ and $V_{ij} = 100\text{--}200 \text{ m s}^{-1}$. The thermal luminosity from the disk L_{th} and the scattered luminosity from the disk L_{sc} depend on the radial optical depth τ and the grain albedo ω : $L_{th}/L_\star = \tau(1 - \omega)(H/2a)$ and $L_{sc}/L_\star = \tau\omega(H/2a)$. The observed range of luminosity ratios, $L_{th}/L_\star \approx L_{sc}/L_\star \approx 10^{-5}$ to 10^{-2} requires $\tau \approx 10^{-3}$ to 1 for $\omega = 0.1\text{--}0.3$ (see also Artymowicz *et al.* 1989; Backman & Paresce 1993; Kenyon *et al.* 1999)

These estimates suggest that collisions of 1 km bodies in a circumstellar disk will yield an observable amount of debris over a disk lifetime of 100 Myr to 1 Gyr. The 1 km planetesimals must have relative velocities of 100 m s^{-1} or more and reside in a disk with an initial mass close to or larger than the minimum mass solar nebula model. We now consider whether gravitational stirring in such a disk allows 1 km bodies to reach such large impact velocities.

3.2. Disks with Single Mass Planetesimals

To understand how gravitational stirring modifies particle velocities in a debris disk, we first consider a small portion of a disk surrounding a 3 M_\odot star. The disk is composed of bodies with a single mass m_0 and a surface density $\Sigma(a) = 0.1 \text{ g cm}^{-2} x (a/70 \text{ AU})^{-3/2}$, where x is a dimensionless constant. A minimum mass solar nebula has $x = 1$ and $\Sigma(70 \text{ AU}) \approx 0.1 \text{ g cm}^{-2}$. We restrict our study to bodies with $r = 1\text{--}100 \text{ km}$; $m_0 = 6.3 \times 10^{15} \text{ g}$ to $6.3 \times 10^{21} \text{ g}$ for icy objects with a mean density of 1.5 g cm^{-3} . Smaller bodies have negligible stirring on cosmological timescales; larger objects are nearly impossible to shatter (KL98; KL99). Each body has $e_0 = 10^{-3}$ and $i_0 = 5 \times 10^{-4}$. We calculate the velocity evolution for $x = 10^{-2}, 10^{-1}, 1$, and 10^1 in model grids composed of 16 annuli with $\delta a/a = 0.001$ and centered at $a_{mid} = 35, 70$, and 140 AU . This study illustrates how viscous stirring modifies planetesimal velocities; dynamical friction occurs only between bodies in adjacent annuli and is small.

Figures 1 and 2 show the evolution of the average particle velocity, $V_i = (h_i^2 + v_i^2)^{1/2}$, and the vertical scale height, $H_i = \sqrt{2}v_i/\Omega_{Ki}$, for the central four annuli of the model grid. A collection of 1 km objects does not evolve in 1 Gyr at 35–140 AU. More massive bodies evolve on an observable timescale. The velocity and scale height for 10 km bodies increase modestly after 1 Gyr, but do not reach the physical conditions needed to begin a collisional cascade (Figure 1). The velocity at 1 Gyr is $V_i(1 \text{ Gyr}) \approx 13 \text{ m s}^{-1} x^{1/4} (a/70 \text{ AU})^{-3/4}$. The scale height of these objects also reaches a small fraction, $\sim 10\%$, of the value needed to reprocess a significant fraction of the stellar luminosity. Calculations with 100 km bodies are more encouraging. In a massive disk, these larger bodies stir themselves rapidly and

reach 100 m s^{-1} velocities on 100 Myr timescales. The velocity at 1 Gyr again depends on a and x , $v(1 \text{ Gyr}) \approx 60 \text{ m s}^{-1} x^{1/4} (a/70 \text{ AU})^{-3/4}$. Thus, in disks with masses at least as large as a minimum mass solar nebula, it is possible to reach velocities of 100 m s^{-1} with gravitational stirring of 100 km bodies.

To test this conclusion further, we consider complete disk models composed of single mass objects. The disk consists of 128 annuli with $\Delta a_i/a_i = 0.0125$, and extends from $a_{in} = 30 \text{ AU}$ to $a_{out} = 150 \text{ AU}$. The surface density of planetesimals is $\Sigma(a) = 0.1(a/70 \text{ AU})^{-3/2} \text{ g cm}^{-2}$, with $e_0 = 10^{-3}$ and $i_0 = 5 \times 10^{-4}$.

Figures 3–4 show the evolution of the velocity and scale height in each disk. A disk with 10 km planetesimals evolves slowly during 1 Gyr. The velocities reach 15% of the shattering velocity; the vertical scale height is sufficient to intercept only $\sim 0.02\%$ of the stellar luminosity (Figure 3). A disk with 100 km planetesimals achieves 100 m s^{-1} velocities over 30–45 AU in 1 Gyr (Figure 4). The scale height is then large enough to intercept 0.1–0.2% of the stellar luminosity. As indicated by the symbols in each panel of Figure 3, the model with 10 km planetesimals yields velocities only $\sim 10\%$ larger than the narrow grid model of Figure 1. This difference grows to $\sim 20\%$ for 100 km planetesimals at 1 Gyr (Figure 4). Long-range stirring produces this velocity difference; large bodies exert more long-range gravitational forces on their distant neighbors than small bodies. Both models produce a power law velocity distribution, $V_i \propto a^{-3/4}$, except at the edges of the grid. The scale height increases slowly with radius, $H_i \propto a^{3/4}$.

Despite fairly rapid stirring of 100 km bodies, it is difficult for these objects to initiate a collisional cascade. The gravitational binding energy of a 100 km object increases the shattering velocity by a factor of 2–3 (equation (4)). Figures 3–4 show that velocities of 200 m s^{-1} cannot be reached in 1 Gyr or less. Thus, a disk composed primarily of planetesimals of a single size cannot undergo a collisional cascade on a timescale of 1 Gyr or smaller.

An obvious and more realistic alternative to this model is a disk composed of objects with a large range of sizes. A set of 100 km bodies can effectively stir up smaller objects on timescales comparable to self-stirring models. These smaller objects can then initiate the collisional cascade. This process would preserve the stirring population, because the large objects are harder to shatter than small objects. We now consider such models to derive the timescale to reach the collisional cascade for a disk with a size distribution of planetesimals.

3.3. Disks with a Size Distribution of Planetesimals

As in the previous section, we begin with the velocity evolution of particles in small portions of a disk containing a size distribution of bodies with radii $r_i = 1 \text{ m}$ to 500 km and surface density $\Sigma(a) = 0.1 \text{ g cm}^{-2} x (a/70 \text{ AU})^{-3/2}$. We assume equal mass in each of 6 mass batches. This mass distribution is a natural outcome of coagulation calculations

(KL99; Kenyon *et al.* 1999). The mass spacing factor between successive batches is $\delta = m_{i+1}/m_i = 10^3$. Each body has $e_0 = 10^{-3}$ and $i_0 = 5 \times 10^{-4}$. We calculate the velocity evolution for $x = 1$ and $x = 10$ in grids of 16 annuli with $\Delta a_i/a_i = 0.001$ centered at $a_{mid} = 35, 70$, and 140 AU. This study illustrates the timescale for dynamical friction to couple with viscous stirring to produce a swarm of small objects with eccentric orbits.

Figure 5 shows the evolution of V_i for small objects in the central four annuli of the model grid. Objects with $r = 1\text{--}1000$ m have nearly identical velocities; larger objects have velocities a factor of two or more smaller. We label each curve with the radius (in km) of the largest object in the mass distribution, r_{max} . The left panels show the velocity evolution for $x = 1$; the right panels show the velocity evolution for $x = 10$. The velocities at 100 Myr to 1 Gyr are

$$V_i(100 \text{ Myr to 1 Gyr}) \approx 25 - 41 \left(\frac{r}{100 \text{ km}} \right)^{0.65} \left(\frac{a}{70 \text{ AU}} \right)^{-0.70} \quad (9)$$

for $x = 1$ and

$$V_i(100 \text{ Myr to 1 Gyr}) \approx 40 - 65 \left(\frac{r}{100 \text{ km}} \right)^{0.65} \left(\frac{a}{70 \text{ AU}} \right)^{-0.70} \quad (10)$$

for $x = 10$. These equations fit the model velocities to 5% or better. Planetesimals with $r \gtrsim 500$ km stir nebular material to the shattering limit in 1 Gyr or less. Smaller planetesimals with $r \sim 200$ km can stir up the inner parts of a massive solar nebula, but cannot stir the outer portions; these planetesimals also fail to stir a minimum mass solar nebula in 1 Gyr or less.

We next consider complete disk models composed of a size distribution of planetesimals. As in §3.1, the disk has 128 annuli with $\Delta a_i/a_i = 0.0125$, and extends from $a_{in} = 30$ AU to $a_{out} = 150$ AU. The surface density of planetesimals is $\Sigma(a) = 0.1(a/70 \text{ AU})^{-3/2} \text{ g cm}^{-2}$, with $e_0 = 10^{-3}$ and $i_0 = 5 \times 10^{-4}$. Disk material is distributed among six mass batches with equal mass per bin and $\delta = 10^3$.

Figures 6–7 show the evolution of the velocity and scale height in disks with $r_{max} = 100$ km (Figure 6) and 500 km (Figure 7). Calculations with $r_{max} = 100$ km produce small objects with velocities at the shattering limit in 1 Gyr. These small bodies are confined to a narrow range of disk radii, $a \lesssim 35\text{--}40$ AU; bodies outside these annuli have much smaller velocities. Calculations with $r_{max} = 500$ km produce small objects with velocities at the shattering limit in roughly 10 Myr at 35 AU, in roughly 100 Myr at 70 AU, and in less than 1 Gyr at 140 AU. The disk with 500 km objects intercepts $\sim 0.1\%$ of the stellar flux at 50–100 Myr; disks with 100 km objects are detectable only after 0.5–1.0 Gyr. As indicated by the symbols in each panel, both of these models produce larger velocity objects compared to the narrow grid models of Figure 5. Long-range stirring produces this velocity

difference. Both models also produce a power law velocity distribution, $V_i \propto a^{-3/4}$, except at the edges of the grid. The scale height increases slowly with radius, $H_i \propto a^{3/4}$, as in the models with single-size planetesimals described above.

To test the sensitivity of the derived timescales to the mass distribution, we calculated model grids with finer mass resolution. Figure 8 shows the velocity evolution for mass distributions at 35 AU with $x = 10$ and $r_{max} = 500$ km. We label each curve in the figure with the mass spacing factor δ . Models with better mass resolution take longer to reach the shattering limit. Because each model has the same dN/dm , models with finer mass resolution have fewer of the largest bodies than models with coarse mass resolution. Thus, our computational procedure produces smaller stirring rates in more finely spaced grids. The difference in the velocity of small particles at 100 Myr as a function of mass spacing is modest: V_i decreases from ~ 190 m s $^{-1}$ for $\delta = 10^3$ to ~ 144 m s $^{-1}$ for $\delta = 5.6$ and ~ 132 m s $^{-1}$ for $\delta = 2$.

3.4. Limitations of the Models

In this paper, we have begun to address some of the limitations and uncertainties of statistical calculations of planetesimal growth in a solar nebula (see KL98 and KL99 for a summary of these limitations). Our multi-annulus code should provide a better treatment of velocity evolution within the nebula, because we calculate short-range and long-range stirring using an evolving density of planetesimals at each radius within the grid. Uncertainties due to the finite spatial resolution and the finite extent of the full grid are small (Figures 3–4, 6–7, and 9). These errors grow when we consider a small portion of a disk, as shown by the symbols in Figures 6–7. Partial disk models with large bodies, $r_{max} \gtrsim 200$ km, have larger uncertainties than models with small bodies, $r_{max} \lesssim 200$ km. Particle velocities are also sensitive to the mass resolution of the grid (Figure 8), but the errors are $\lesssim 50\%$ for any mass resolution, $\delta \lesssim 10^3$. Larger errors are possible when the calculations include mergers and fragmentation (see KL98, KL99, and references therein). We plan to examine this issue for the multi-annulus evolution code in a future paper.

Our conclusions concerning the long term evolution of particle velocities are probably insensitive to our neglect of important physical processes, such as mergers with fragmentation and radiative processes such as Poynting-Robertson drag. The timescale to produce 100–1000 km objects in a solar nebula is generally short compared to the stirring time (KL99; Kenyon *et al.* 1999). Our assumption of an initial population of 100–500 km objects therefore does not lead to a large uncertainty in the stirring timescale. Previous calculations have also shown that collisions tend to redistribute kinetic energy from the larger bodies to the smaller bodies (KL99). Including this process in the calculations would probably reduce stirring times by 25% to 50%. Calculations with the better mass resolution

needed to follow mergers and fragmentation tend to increase stirring times by a similar factor (Figure 8). Thus, a more accurate treatment with better mass resolution which includes mergers and fragmentation will probably yield stirring times close to those derived here.

Our neglect of processes which remove particles from the grid probably also has little impact on the derived stirring timescales. Gas drag removes few of the 1 km objects needed for the collisional cascade and has negligible impact on their velocities (KL99). Poynting-Robertson drag and ejection by radiation pressure are important for small particles once the collisional cascade begins (Burns *et al.* 1979; Backman, Dasgupta, & Stencel 1995). We have concentrated on the evolution leading up to the collisional cascade and plan to consider the cascade itself in a future paper.

Finally, our stirring timescales are upper limits for debris disks containing larger objects with radii exceeding 1000 km. Estimating stirring timescales for these objects using the approach in this paper is difficult, because the growth rate of large objects is comparable to the stirring timescale in the outer disk (KL99; Kenyon *et al.* 1999). The statistical approach used for these calculations also begins to break down when the most massive objects are few in number, although Weidenschilling *et al.* (1997) note that the stirring rates for one large body are remarkably close to those derived from complete n -body calculations (see the Appendix). Our approach also does not include orbital resonances, which become important for planets with masses much larger than those considered here. We suspect that the stirring timescales for objects with radii of 1000–3000 km will roughly follow the scaling laws described in §3.3, but cannot confirm this hypothesis without a more sophisticated calculation.

We conclude that our stirring times are reasonably accurate estimates for a debris disk containing a mass distribution of modest-sized planets and planetesimals with $r \lesssim 500$ km.

Future calculations including coagulation and shattering will yield predicted surface density distributions for the dust in a model disk. In the stirring calculations described here, we adopt an initial surface density distribution $\Sigma \propto r^{-3/2}$ which remains fixed with time. Surface density distributions derived from observations range from $\Sigma \propto r^{-1}$ (e.g., Wilner *et al.* 2000) to $\Sigma \propto r^{-3}$ (e.g., Trilling *et al.* 2000). Tests with different surface density distributions suggest that the radial velocity gradient becomes flatter as the surface density distribution becomes shallower. We thus expect larger velocities and larger scale heights in disks with more mass at larger distances from the central star. The exponent in the radial surface density distribution may well evolve with time, because the timescales to produce large planets in the disk is a strong function of heliocentric distance (Kenyon *et al.* 1999).

Our simple models do not explain isolated features observed in debris disks such as gaps, warps, and other asymmetries. Gaps and perhaps warps are a natural outcome of

large planet formation in the disk (see Artymowicz 1997 and references therein). The size of the gap surrounding a large planet with mass M_P is roughly 5–10 Hill radii, where $R_H \sim (M_P/3M_\star)^{1/3}$ (see the Appendix and references therein). Large planets can cause gaps and rings through mean motion resonances; the size of the gap or ring produced by a resonance also depends on R_H (e.g., Holman & Wisdom 1993). Bright spots in a disk or ring might be caused by a planet which forces eccentric orbits (Wyatt *et al.* 1999). More sophisticated treatments of planetary dynamics, such as n -body simulations, are needed to understand the formation and evolution of these features. The coagulation and gravitational stirring models described here and in KL99 will eventually yield plausible initial conditions for n -body simulations.

4. DISCUSSION AND SUMMARY

On timescales of 10 Myr to 1 Gyr, disks with a size distribution of planetesimals can reach conditions needed to produce a collisional cascade. In this model, large bodies stir up small bodies to large velocities; collisions between smaller bodies initiate the collisional cascade. In our calculations with equal mass per mass bin, the disk must be at least as massive as a minimum mass solar nebula and contain objects with radii of 500 km or larger. Larger objects in massive disks stir the velocities of small planetesimals more effectively than smaller objects in less massive disks.

Once the collisional cascade begins, a simple estimate using the coagulation equation indicates that the survival time for the disk is roughly 500 Myr for a minimum mass solar nebula with a size of 100 AU composed primarily of 1 km objects. More massive disks have shorter survival times, because the coagulation timescale is inversely proportional to the initial mass in the disk (see KL98 and KL99). Smaller disks also have shorter survival times. This estimate is probably accurate to a factor of 2–3 based on previous, more complete coagulation calculations in a single annulus (KL99; Kenyon *et al.* 1999). Multi-annulus coagulation calculations now underway will test this estimate in more detail.

Our results account for several observed aspects of nearby protostellar disks. The estimated disk lifetime of ~ 500 Myr agrees with the median age of ~ 400 Myr for the central stars of debris disk systems derived from *ISO* and other data (e.g., Habing *et al.* 1999). A coagulation model can account for the large range in central star ages, ~ 10 Myr for HR 4796A up to ~ 1 Gyr for 55 Cnc, by varying the initial mass of the disk. In our interpretation, the disks in young systems such as HR 4796A are initially more massive than the disks in older stars such as 55 Cnc. Song *et al.* (2000) note that the median age is larger for less massive stars with debris disks. A coagulation model naturally explains this observation, because the collision time scales with the orbital timescale, $\tau_{orb} \propto M_\star^{-1/2}$. Future studies with *SOFIA* and *SIRTF* should yield larger samples of systems to test the

predicted lifetimes as a function of stellar mass and the initial mass in the disk.

The observed scale height profiles of debris disk systems place useful constraints on coagulation and stirring models. The predicted scale height distribution $H \propto r^{3/4}$ is shallower than the typical distribution observed in β Pic and other systems $H \propto r$ (e.g., Artymowicz 1997, Lagrange *et al.* 2000). Radiation pressure on shattered grains in the inner portions of the disk should increase the scale height at larger radii; Poynting-Robertson drag on shattered grains in the outer parts of the disk should decrease the scale height at small radii. Coagulation tends to produce larger objects in the inner portions of the disk and should produce larger scale heights in the inner disk. Although more detailed calculations are needed to see how these competing physical processes act on the observed scale height, we are encouraged that the scale height distribution derived solely from the stirring calculations is close to those observed in real debris disk systems.

We acknowledge a generous allotment of computer time on the HP Exemplar ‘Neptune’ and the Silicon Graphics Origin-2000 ‘Alhena’ through funding from the NASA Offices of Mission to Planet Earth, Aeronautics, and Space Science.

A. APPENDIX

A.1. Overview

We assume that planetesimals are a statistical ensemble of masses in N concentric, cylindrical annuli with width Δa_i , and height H_i centered at radii a_i from a star with mass M_\star and luminosity L_\star . The particles have horizontal $h_{ik}(t)$ and vertical $v_{ik}(t)$ velocity dispersions relative to an orbit with mean Keplerian velocity V_{Ki} (see Lissauer & Stewart 1993). We approximate the continuous distribution of particle masses with discrete batches having an integral number of particles $n_{ik}(t)$ and total masses $M_{ik}(t)$. The average mass of each of M mass batches, $m_{ik}(t) = M_{ik}(t)/n_k(t)$, evolves with time as collisions add and remove bodies from the batch (Wetherill & Stewart 1993).

KL98 and KL99 describe our approach for solving the evolution of particle numbers and velocities for a mass batch k in a single annulus i during a time step δt . Here we generalize the velocity evolution from elastic collisions for a set of annuli. Interactions occur between particles with masses m_{ik} in annulus i and m_{jl} in annulus j . Each annulus has a geometric width Δa_i . Annuli with a fixed constant size have $\Delta a_i = a_{i+1} - a_i$. Annuli with a variable width have $\Delta a_i = \Delta a_0 \cdot a_i$ and $a_i = a_{in}((1 + 0.5\Delta a_0)/(1 - 0.5\Delta a_0))^i$, where a_{in} is the inner edge of the first annulus. Following Weidenschilling *et al.* (1997), particles interact if their orbits approach within 2.4 times their mutual Hill radius R_H . The ‘overlap region’ for elastic collisions is

$$o_{ijkl,el} = 2.4R_H + 0.5(w_{ik} + w_{jl}) - |a_i - a_j|; \quad (A1)$$

where w_{ik} is the radial extent of the orbit of particle k with orbital eccentricity e_k in annulus i :

$$w_{ik} = \begin{cases} \Delta a_i + e_k a_i & e_k a_i \leq \Delta a_i \\ (\Delta a_i + e_k a_i)(e_k a_i / \Delta a_i)^{1/4} & e_k a_i > \Delta a_i \end{cases} \quad (A2)$$

A.2. Velocity Evolution

We solve a set of Fokker-Planck equations to follow the time-evolution of h_{ik} and v_{ik} (Hornung *et al.* 1985; Wetherill & Stewart 1993; Stewart & Ida 2000):

$$\frac{dh_{vs,ik}^2}{dt} = \sum_{j=1}^{j=N} \sum_{l=1}^{l=M} f_{ij} C (h_{ik}^2 + h_{jl}^2) m_{jl} B_\Lambda J_e(\beta) \quad (A3)$$

$$\frac{dv_{vs,ik}^2}{dt} = \sum_{j=1}^{j=N} \sum_{l=1}^{l=M} f_{ij} \frac{C}{\beta_{kl}^2} (v_{ik}^2 + v_{jl}^2) m_{jl} B_\Lambda J_z(\beta) \quad (A4)$$

for viscous stirring and

$$\frac{dh_{df,ik}^2}{dt} = \sum_{j=1}^{j=N} \sum_{l=1}^{l=M} f_{ij} C (m_{jl} h_{jl}^2 - m_{ik} h_{ik}^2) A_\Lambda H_e(\beta) \quad (A5)$$

$$\frac{dv_{df,ik}^2}{dt} = \sum_{j=1}^{j=N} \sum_{l=1}^{l=M} f_{ij} \frac{C}{\beta_{kl}^2} (m_{jl} v_{jl}^2 - m_{ik} v_{ik}^2) A_\Lambda H_z(\beta) \quad (A6)$$

for dynamical friction. In these expressions, N is the number of annuli and M is the number of mass batches within each annulus; $\beta_{kl}^2 = (i_{ik}^2 + i_{jl}^2)/(e_{ik}^2 + e_{jl}^2)$, and $C = G^2 \rho_l / (\sqrt{\pi} V_K^3 (h_{ik}^2 + h_{jl}^2)^{3/2})$ is a function of the density of particles in batch l and the relative horizontal velocity of the mass batches (Wetherill & Stewart 1993, Stewart & Ida 2000). The functions H_e , H_z , J_e , and J_z are definite integrals defined in Stewart & Ida (2000). The overlap fraction f_{ij} is the fraction of bodies in annulus i that approach within $2.4 R_H$ of the bodies in annulus j . We set $\rho_l = M_l/V_l$, where M_l is the total mass of bodies with m_l in annulus j and V_l is the larger of the two volumes for the interacting annuli. Following Stewart & Ida (2000), we also set $A_\Lambda = \ln(\Lambda^2 + 1)$ and $B_\Lambda = A_\Lambda - \Lambda^2/(\Lambda^2 - 1)$, where

$$\Lambda = \left(\frac{m_{ik} + m_{jl}}{M_\star} \right)^{-1} \left(\frac{H_{ijkl}}{a_{avg}} + \frac{R_H}{a_{avg}} \right) V_{ij}^2, \quad (A7)$$

is for calculations without physical collisions and

$$\Lambda = \left(\frac{H_{ijkl} + G(m_{ik} + m_{jl})V_{ij}^{-2}}{(r_{ik} + r_{jl})(1 + 2(V_{e,ij}/V_{ij})^2)} \right), \quad (A8)$$

is for calculations with physical collisions. In these expressions, G is the gravitational constant, H_{ijkl} is the mutual scale height, $a_{avg} = 0.5(a_i + a_j)$, and R_H is the mutual Hill radius, $R_H = ((m_{ik} + m_{jl})/3 M_\star)^{1/3} a_{avg}$.

This formulation for velocity evolution breaks down in the low velocity regime, when the relative velocities of particles approach the Hill velocity, $v_H = R_H V_K / a$. KL99 described a simple solution to this problem, based on a comparison of N -body integrations (Ida 1990) with published scaling laws for velocity evolution at low velocities (Barge & Pellat 1991; Wetherill & Stewart 1993; Weidenschilling *et al.* 1997). This solution fails at very low velocities. We thus replaced equations (A20) and (A21) of KL99 with the more accurate results of Ida & Makino (1992, 1993):

$$\left(\frac{dh_{vs,ik}^2}{dt} \right)_{lv} = \sum_{j=1}^{j=N} \sum_{l=1}^{l=M} C'_{h,vs} \left(\frac{G^2}{m_{ik} + m_{jl}} \right)^{2/3} \rho_{jl} m_{jl} H_{jl} \Omega_{ij}^{1/3} \quad (A9)$$

$$\left(\frac{dv_{vs,ik}^2}{dt} \right)_{lv} = \sum_{j=1}^{j=N} \sum_{l=1}^{l=M} C'_{i,vs} \left(\frac{G}{(m_{ik} + m_{jl})^2} \right)^{2/3} \Omega_{ij}^{-1/3} \rho_{jl} m_{jl} H_{jl} (v_{ik}^2 + v_{jl}^2) \quad (\text{A10})$$

for viscous stirring and

$$\left(\frac{dh_{df,ik}^2}{dt} \right)_{lv} = \sum_{j=1}^{j=N} \sum_{l=1}^{l=M} C'_{e,df} \left(\frac{\Omega_{ij} R_H^2 \rho_{jl} H_{ijkl}}{m_{ik} m_{jl}} \right) (m_{jl} h_{jl}^2 - m_{ik} h_{ik}^2) \quad (\text{A11})$$

$$\left(\frac{dv_{df,ik}^2}{dt} \right)_{lv} = \sum_{j=1}^{j=N} \sum_{l=1}^{l=M} C'_{i,df} \left(\frac{\Omega_{ij} R_H^2 \rho_{jl} H_{ijkl}}{m_{ik} m_{jl}} \right) (m_{jl} v_{jl}^2 - m_{ik} v_{ik}^2) \quad (\text{A12})$$

for dynamical friction. In these expressions, Ω_{ij} is the average angular frequency of the two Keplerian orbits, and H_{jl} is the vertical scale height of particles in annulus l . The C 's are constants: $C'_{h,vs} = 10$, $C'_{v,vs} = 1$, and $C'_{h,df} = C'_{v,df} = 5$. We adjusted the values of these to agree with results of n -body calculations described below.

The Fokker-Planck equations – and their low velocity substitutes – do not include stirring rates for distant perturbations of particles whose orbits do not cross. Weidenschilling (1989) and Hasegawa & Nakazawa (1990) derived expressions for the rate of change of orbital eccentricities and inclinations for distant encounters. Stewart & Ida (2000) show that these perturbation calculations underestimate the strength of distant encounters when the orbital separation is smaller than several R_H . They derive expressions appropriate for velocity evolution in a single annulus and show that their results agree with n -body simulations. We follow Weidenschilling *et al.* (1997) and use the stirring rates defined in Weidenschilling (1989). These are:

$$\frac{dh_{lr,ik}^2}{dt} = \sum_{j=1}^{j=N} \sum_{l=1}^{l=M} C_{lr,e} x_{ij} \frac{G^2 \rho_{jl} M_{jl}}{\Omega_{avg}} \left(\frac{\tan^{-1}(H_{ijkl}/D_{min})}{D_{min}} - \frac{\tan^{-1}(H_{ijkl}/D_{max})}{D_{max}} \right) \quad (\text{A13})$$

for continuum bodies and

$$\frac{dh_{lr,ik}^2}{dt} = \sum_{j=1}^{j=N} \sum_{l=1}^{l=M} \frac{G^2}{\pi \Omega a} \left(\frac{C'_{lr,e} m_l^2}{(\delta a^2 + 0.5 H_{jl}^2)^2} \right) \quad (\text{A14})$$

where $D_{min} = \max(2.4R_H, 1.6(h_{ik}^2 + h_{jl}^2)^{1/2})$, $D_{max} = 0.5 \max(w_{ik}, w_{jl})$, and $\delta a = |a_i - a_j|$. We do not calculate long-range stirring rates for inclination, because these rates are much smaller than rates for the eccentricity (Weidenschilling 1989; Stewart & Ida 2000). These equations, together with equations (A9)–(A12), yield satisfactory agreement between our

calculations and the results of more accurate direct n -body integrations for $C_{lr,e} = 23.5$ and $C'_{lr,e} = 5.9$ (see below). Our choices for the constants in these expressions are larger than those of Weidenschilling (1989) to mimic the increased long-range stirring derived by Stewart & Ida (2000).

To solve the set of coagulation and velocity evolution equations, we employ a fourth order Runge-Kutta solution (Press *et al.* 1992). For each timestep, we derive separate solutions for a full timestep of length δt and for two half timesteps of length $\delta t/2$. These solutions converge if the maximum difference between the dynamical variables is $\delta_{err} < \delta_{max}$; we adopt $\delta_{max} = 10^{-5}$ for most calculations. We follow Press *et al.* (1992) and increase the timestep by $(\delta_{err}/\delta_{max})^{0.20}$ when the solution converges and decrease the timestep by $(\delta_{err}/\delta_{max})^{0.25}$ when the solution does not converge.

Our algorithm evolves quantities which lie in bins of radius, a discretization which provides a good starting point for parallel computation. We use explicit message-passing functions to distribute the summations required in the evolution equations to multiple processors. Each processor handles a unique set of radial bins and performs summations only for those indices. The computations depend on access to information from all radial bins, hence prior to each time step, we communicate the state of quantities in all bins to all processors. For the number of processors we use, up to 32 on an HP Exemplar and an SGI Origin 2000, this communication load is not great and the algorithm speeds up nearly linearly with the number of processors.

A.3. Tests of the Evolution Code

To test the velocity evolution algorithm, we attempt to reproduce published n -body and particle-in-a-box calculations. Stewart & Ida (2000), Ida & Makino (1993), and Kokubo & Ida (1995) describe n -body calculations of gravitational stirring of planetesimals in orbit at 1 AU; Weidenschilling *et al.* (1997) and Stewart & Ida (2000) show that particle-in-a-box calculations roughly match the n -body results.

We begin with tests of the ‘standard’ velocity evolution algorithm in the high velocity limit. Stewart & Ida (2000) describe several comparisons of stirring calculations in a single annulus with detailed n -body calculations. Here we try to reproduce the n -body results using a collection of N annuli. The first test considers 800 planetesimals with masses $m_1 = 10^{24}$ g orbiting the Sun at $a_0 = 1$ AU. These bodies are evenly distributed on a grid with inner radius $a_{in} = a_0 - 40R_H$ and outer radius $a_{out} = a_0 + 40R_H$; R_H is the Hill radius for collisions between these bodies, $R_H = 0.0007$ AU. We consider grids with 20, 40, and 80 annuli to test the sensitivity of the results to the grid spacing. The surface density is $\Sigma = 10$ g cm⁻². The bodies have $e_0 = 2i_0 = 2 \times 10^{-3}$.

Figure 9 shows that the evolution of e and i is independent of the grid spacing. We plot

e and i in units of the Hill radius for the central four annuli of the model grid. Our results are nearly identical to the n -body calculations of Stewart & Ida (2000). At 20,000 yr, our result for e is $\sim 5\%$ smaller than the Stewart & Ida result; our value for i is indistinguishable from the Stewart & Ida result. The small difference in the eccentricity evolution probably results from long range stirring; Stewart & Ida (2000) use another algorithm for long-range stirring which is more computationally expensive and probably more accurate than the one we use here.

Figure 10 shows the radial profile of the velocity distribution at three points in the evolution. The velocity profiles become more bow-shaped at late times, because objects at the edges of the grid have fewer neighbors than objects in the middle of the grid. The shape of this bow is independent of the grid spacing, as indicated by the dot-dashed and dashed lines in Figure 10.

Figure 11 compares the results of the first test with two other tests described by Stewart & Ida (2000). These tests follow the evolution of (a) 8000 planetesimals with $m_1 = 10^{24}$ g with a surface density of 100 g cm^{-2} and (b) 400 planetesimals with $m_1 = 10^{26}$ g and a surface density of 500 g cm^{-2} . For another comparison, we consider (c) 4×10^5 planetesimals with $m_1 = 10^{23}$ g and the same surface density as (b). Stewart & Ida (2000) demonstrated that the time evolution of these tests scales with the mass of a planetesimal and the surface density as

$$\frac{de}{dt} \propto \left(\frac{\sigma}{10 \text{ g cm}^{-2}} \right) \left(\frac{10^{24} \text{ g}}{m_1} \right)^{1/3} \frac{de_H}{dt'} \quad (\text{A15})$$

$$\frac{di}{dt} \propto \left(\frac{\sigma}{10 \text{ g cm}^{-2}} \right) \left(\frac{10^{24} \text{ g}}{m_1} \right)^{1/3} \frac{di_H}{dt'} , \quad (\text{A16})$$

where t' is a scaled time. The dashed and dot-dashed curves in Figure 11 show the scaled evolution for tests (a), (b), and (c). There is excellent agreement between these results and the time evolution of the eccentricity and inclination shown in Figure 9: the models with $m_1 = 10^{23}$ g lag test (a) by $\sim 1\%$ throughout the evolution, while models with $m_1 = 10^{26}$ g run ahead by $\sim 1\%$.

To test the low velocity limit of the multi-annulus code, we consider a calculation of $N = 805$ planetesimals with masses $m_1 = 2 \times 10^{24}$ g orbiting the Sun at $a_0 = 1 \text{ AU}$. The planetesimals are evenly distributed on a grid with inner radius $a_{in} = a_0 - 17.5R_H$ and outer radius $a_{out} = a_0 + 17.5R_H$; R_H is the Hill radius for collisions between m_1 and $m_2 = 2 \times 10^{26}$ g, $R_H = 0.003235 \text{ AU}$. The 35 annuli in this grid are spaced at intervals of R_H . The surface density is $\Sigma = 10 \text{ g cm}^{-2}$. The bodies have $e_0 = i_0 = 3.235 \times 10^{-5}$.

Figure 12 shows the time evolution of $(e^2 + i^2)$ for these bodies in units of the Hill radius. The velocities of all planetesimals increase uniformly with time; the average

eccentricity is $e \approx 0.7R_H$ at $t = 100$ yr, $e \approx 1.27R_H$ at $t = 800$ yr, and $e \approx 1.63R_H$ at $t = 2000$ yr. Particles at the edge of the grid have somewhat smaller velocities, because they do not have as many neighbors. The dashed line in the Figure plots the eccentricity evolution for a model grid with 70 annuli spaced at intervals of R_H ; the difference between this model and the ‘standard’ grid with 35 annuli is small.

Figure 13 shows how the 2×10^{24} g planetesimals react when a single object with $m_2 = 2 \times 10^{26}$ g lies at a_0 . Velocities of small planetesimals within $\pm 3\text{--}4 R_H$ of the larger planetesimal increase rapidly due to short range stirring. Velocities of more distant planetesimals increase slowly due to long range stirring by the large planetesimal and short range stirring by nearby small planetesimals. The radial profile of the velocity distribution for the central 9 annuli is fairly flat at $t = 2000$ yr, and has a similar amplitude and shape as the velocity distribution for an n -body calculation with identical starting parameters (see Ida & Makino 1993). Our calculation yields fewer annuli in the central high velocity peak compared to the n -body calculation. Planetesimals in the center of the n -body grid migrate away from the massive object and then stir up planetesimals farther out in the grid; our algorithm does not include this evolution. Weidenschilling *et al.* (1997) obtained results similar to ours.

Figures 14 and 15 show the evolution of the planetesimal swarm when another large planetesimal is added. The two large planetesimals at $\pm 5R_H$ in Figure 14 initially interact only by long range stirring; the early evolution of small planetesimals near each of the large planetesimals thus follows the evolution shown in Figure 13. Once the orbits near the two large bodies begin to cross, the velocities of the smaller planetesimals increase more rapidly than those near a single large body. The velocity profile is still flat at $t = 2000$ yr; the area of the high velocity peak is roughly twice the area of the high velocity peak in Figure 13.

The two large planetesimals at $\pm 2R_H$ in Figure 15 interact by short range stirring throughout the evolution. Small planetesimals rapidly increase in velocity and reach $(e^2 + i^2)^{1/2} \approx 5.5 R_H$ in 2000 yr. The velocities of the large planetesimals increase as well and approach $(e^2 + i^2)^{1/2} \approx 2 R_H$ at the end of the test. Our results for the small planetesimals agree well with the n -body results of Kokuba & Ida (1995) and the multizone calculations of Weidenschilling *et al.* (1997). The evolution of the larger bodies in our calculations is also similar to those of other calculations for large initial separations (as in Figure 14). We do not treat short-range interactions as well as other calculations that follow the actual orbits of larger bodies.

Finally, Figure 16 shows the results of a calculations with 8 large planetesimals, $m_2 = 2 \times 10^{26}$ g, embedded in a uniform sea of 805 smaller bodies with $m_1 = 2 \times 10^{24}$ g. As in Kokubo & Ida (1995) and Weidenschilling *et al.* (1997), the small bodies achieve large velocities, $(e^2 + i^2)^{1/2} \approx 6.5 R_H$ in 2000 yr. The shape and amplitude of our radial distribution of $(e^2 + i^2)^{1/2}$ agrees well with previous results. The velocities of the large

bodies increase uniformly as well and reach $(e^2 + i^2)^{1/2} \approx 3 R_H$ at the end of the evolution. The velocities of the large bodies in Figure 16 agree with the median velocity of bodies in the Kokubo & Ida (1995) and the Weidenschilling *et al.* (1997) calculations. Our calculations do not display the same chaotic behavior as these more detailed calculations, because we do not follow individual orbits for the large bodies.

We conclude that our multi-annulus planetesimal evolution code matches a variety of tests reasonably well. The code successfully follows the evolution of large numbers of interacting planetesimals with a range of masses. The code also successfully calculates the velocity evolution of small numbers of large planetesimals when close interactions are unimportant. Our code does not account for the chaotic behavior of these close encounters, but it does yield reasonably good velocities averaged over several close encounters. We plan to consider better treatments of these ‘one-on-one’ interactions in a future study.

REFERENCES

Artymowicz, P., Burrows, C., & Paresce, F. 1989, ApJ, 337, 494

Artymowicz, P. 1997, ARE&PS, 25, 175

Augereau, J. C., Lagrange, A.-M., Mouillet, D., & Ménard, F. 1999, A&A, 350, L51

Augereau, J. C., Lagrange, A.-M., Mouillet, D., Papaloizou, J. C. B., & Grorod, P. A. 1999, A&A, 348, 557

Backman, D. E., Dasgupta, A., & Stencel, R. E. 1995, ApJ, 450, L35

Backman, D. E., & Paresce, F. 1993, in *Protostars and Planets III*, eds. E. H. Levy & J. I. Lunine, Tucson, Univ of Arizona, p. 1253

Barge, P., & Pellat, R. 1991, Icarus, 93, 270

Barrado y Navascués, D., Stauffer, J. R., Hartmann, L., & Balachandran, S. C. 1997, ApJ, 475, 313

Barrado y Navascués, D., Stauffer, J. R., Song, I., & Caillault, J.-P. 1999, ApJ, 520, L123

Becklin, E., E., Silverstone, M., Chary, R., Hare, J., Zuckerman, B., Spangler, C., & Sargent, A. 1998, Ap&SS, 255, 113

Burns, J. A., Lamy, P. L., & Soter, S. 1979, Icarus, 40, 1

Davis, D. R., Chapman, C. R., Weidenschilling, S. J., & Greenberg, R. 1985, Icarus, 62, 30

Davis, D. R., Ryan, E. V., & Farinella, P. 1994, Planet. Space Sci., 42, 599

Dent, W. R. F., *et al.* 1995, MNRAS, 277, L25

Dominik, C., *et al.* 1998, Ap&SS, 255, 103

Fajardo-Acosta, S. B., Stencel, R. E., & Backman, D. E. 1997, ApJ, 487, L151

Fajardo-Acosta, S. B., Stencel, R. E., Backman, D. E., & Thakur, N. 1999, ApJ, 520, 215

Gaidos, E. J. 1999, ApJ, 510, L131

Greaves J. S., Coulson, I. M., & Holland, W. S. 2000a, MNRAS, 312, L1

Greaves, J. S. *et al.* 1998, ApJ, 506, L133

Greaves J. S., Mannings V. & Holland, W. S. 2000b, Icarus, 143, 155

Habing, H. J., *et al.* 1999, *Nature*, 401, 456

Hasegawa, M., & Nakazawa, K. 1990, *A&A*, 227, 619

Hayashi, C. 1981, *Prog Theor Phys Suppl*, 70, 35

Holland, W. S., *et al.* 1998, *Nature*, 392, 788

Holman, M. J., & Wisdom, J. 1993, *AJ*, 105, 1987

Hornung, P., Pellat, R., & Barge, P. 1985, *Icarus*, 64, 295

Ida, S. 1990, *Icarus*, 88, 129

Ida, S., Larwood, J., & Burkert, A. 2000, *ApJ*, 528, 351

Ida, S., & Makino, J. 1992, *Icarus*, 96, 107

Ida, S., & Makino, J. 1993, *Icarus*, 106, 210

Jayawardhana, R. *et al.* 2000, *ApJ*, in press

Jayawardhana, R. *et al.* 1998, *ApJ*, 503, L79

Kalas, P., Larwood, J., Smith, B. A., & Schultz, A. 2000, *ApJ*, 530, L133

Kenyon, S. J., & Luu, J. X. 1998, *AJ*, 115, 2136 (KL98)

Kenyon, S. J., & Luu, J. X. 1999, *AJ*, 118, 1101 (KL99)

Kenyon, S. J., Wood, K., Whitney, B. A., & Wolff, M. 1999, *ApJ*, 524, L119

Koerner, D. W., Ressler, M. E., Werner, M. W., & Backman, D. E. 1998, *ApJ*, 503, L83

Kokubo, E., & Ida, S. 1995, *Icarus*, 114, 247

Kokubo, E., & Ida, S. 1996, *Icarus*, 123, 180

Lagrange, A.-M., Backman, D., & Artymowicz, P. 2000, in *Protostars & Planets IV*, eds. V. Mannings, A. P. Boss, & S. S. Russell, Tucson, Univ. of Arizona, in press

Lecavelier des Etangs, A., Vidal-Madjar, A., & Ferlet, R. 1998, *A&A*, 328, 602

Lissauer, J. J., & Stewart, G. R. 1993, In *Protostars and Planets III*, edited by E. H. Levy and J. I. Lunine, U. of Arizona Press, Tucson, 1061

Mouillet, D., Larwood, J. D., Papaloizou, J. C. B., & Lagrange, A.-M. 1997, *MNRAS*, 292, 896

Press, W. H., Flannery, B. P., Teukolsky, S. A., & Vetterling, W. T. 1992, *Numerical Recipes, The Art of Scientific Computing*, Cambridge, Cambridge

Safronov, V. S. 1969, Evolution of the Protoplanetary Cloud and Formation of the Earth and Planets, Nauka, Moscow [Translation 1972, NASA TT F-677]

Schneider, G., *et al.* 1999, ApJ, 513, L127

Song, I., Caillault, J.-P., Barrado y Navascués, D., Stauffer, J. R., & Randich, S. 2000, ApJ, 533, L41

Spaute, D., Weidenschilling, S. J., Davis, D. R., & Marzari, F. 1991, Icarus, 92, 147

Stern, S. A. 1995, AJ, 110, 856

Stern, S. A. 1996, AJ, 112, 1203

Stewart, G. R., & Ida, S. 2000, Icarus, 143, 28

Trilling, D. E., & Brown, R. H. 1998, Nature, 395, 775

Trilling, D. E., Brown, R. H., & Rivkin, A. S. 2000, ApJ, 529, 499

Weidenschilling, S. J. 1977, *Astrophys Sp Sci*, 51, 153

Weidenschilling, S. J., Spaute, D., Davis, D. R., Marzari, F., & Ohtsuki, K. 1997, Icarus, 128, 429

Wetherill, G. W., & Stewart, G. R. 1993, Icarus, 106, 190

Wilner, D. J., Ho, P. T. P., Kastner, J. H., & Rodriguez, L. F. 2000, ApJ, 534, L101

Wyatt, M. C., Dermott, S. F., Telesco, C. M., Fisher, R. S., Grogan, K., Holmes, E. K., & Piña, R. K. 1999, ApJ, 527, 918

Zuckerman, B., Forveille, T., & Kastner, J. H. 1995, Nature, 373, 494

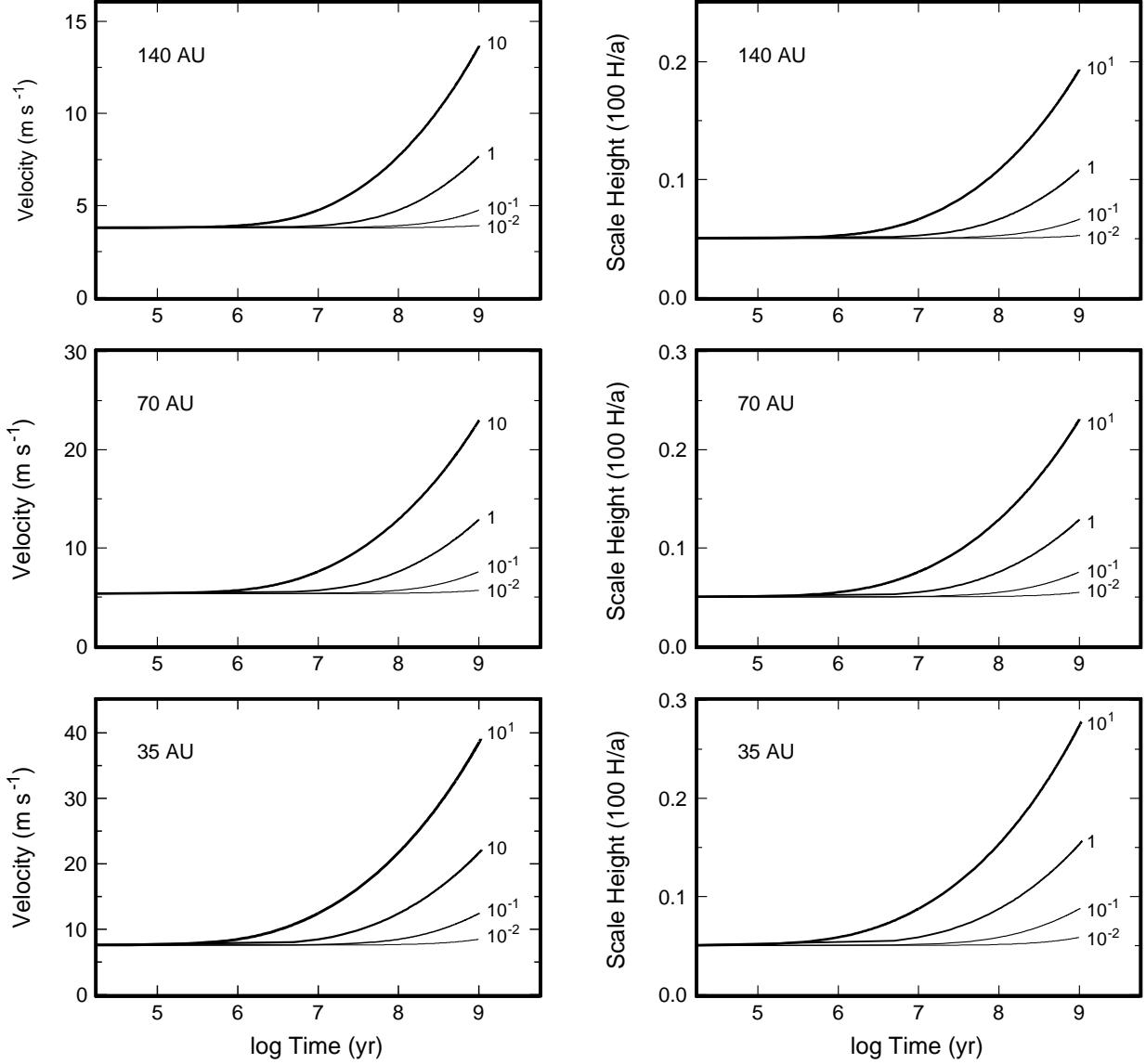


Fig. 1.— Evolution of particle velocity (left panels) and vertical scale height (right panels) for 10 km planetesimals in orbit around a $3 M_{\odot}$ star at 35 AU (lower panels), 70 AU (middle panels), and 140 AU (top panels). The four curves in each panel show the evolution for planetesimals with normalized surface densities, x , indicated to the right of each curve. Models with $x = 1$ have a surface density of solids comparable to that in the minimum mass solar nebula.

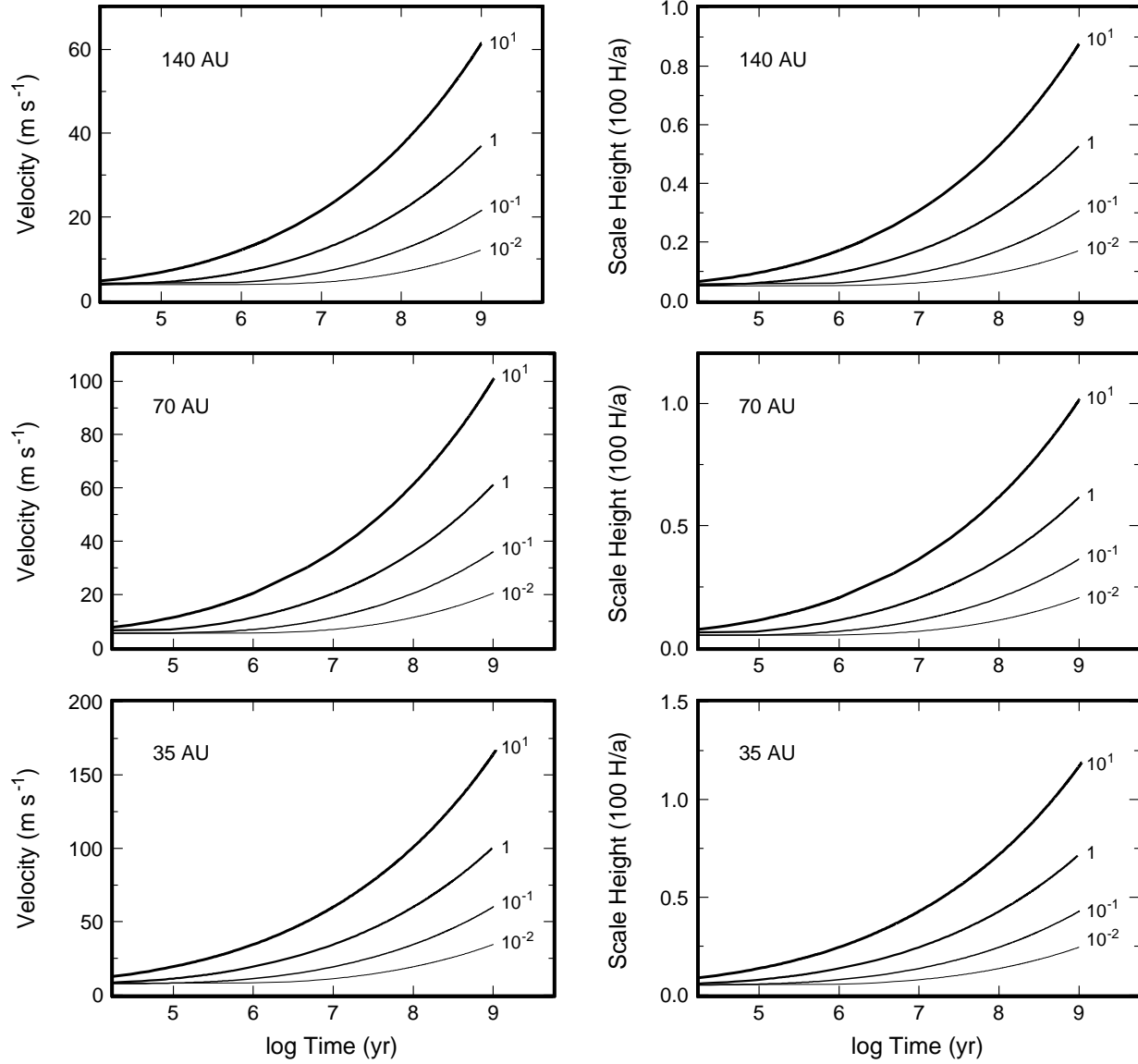


Fig. 2.— As in Figure 1, for 100 km planetesimals.

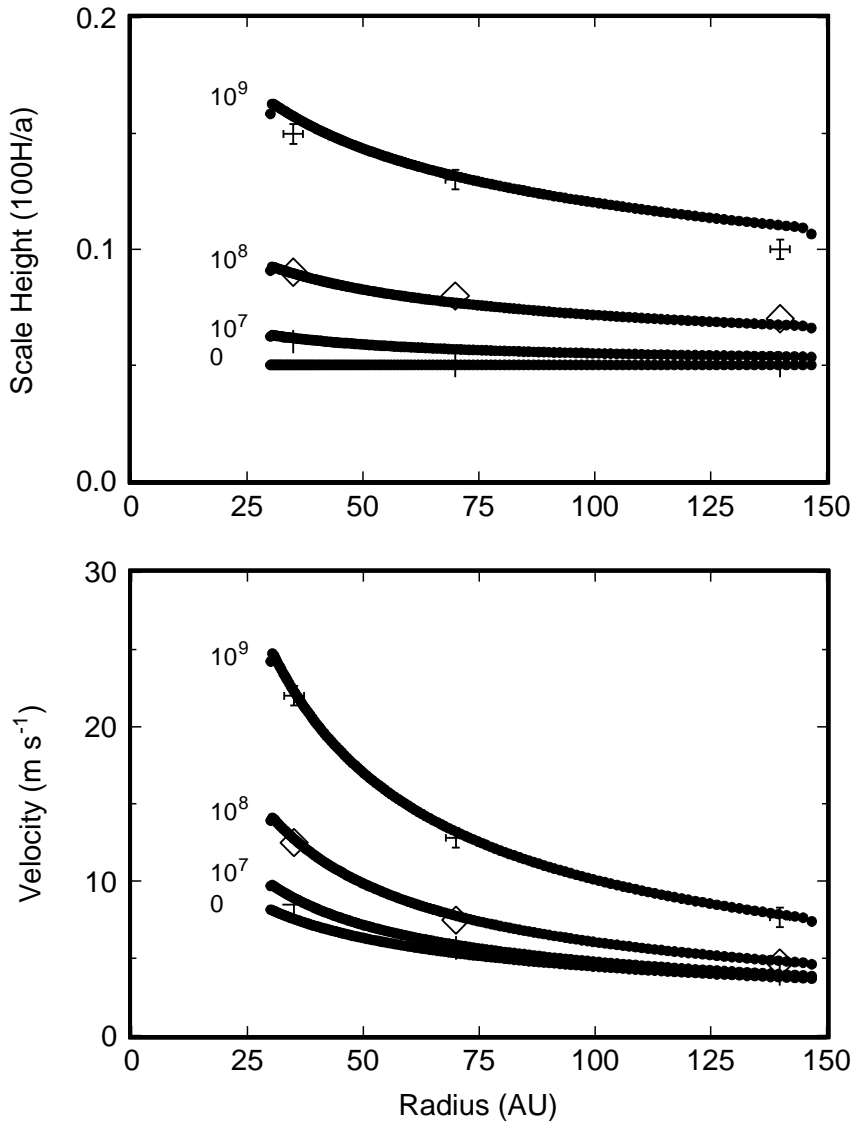


Fig. 3.— Evolution of particle velocity (lower panel) and vertical scale height (top panel) for 10 km planetesimals in a disk surrounding a $3 M_{\odot}$ star. The initial surface density in the disk is $\Sigma = 60(a/1 \text{ AU})^{-3/2}$. The evolution time in years is listed to the left of each curve.

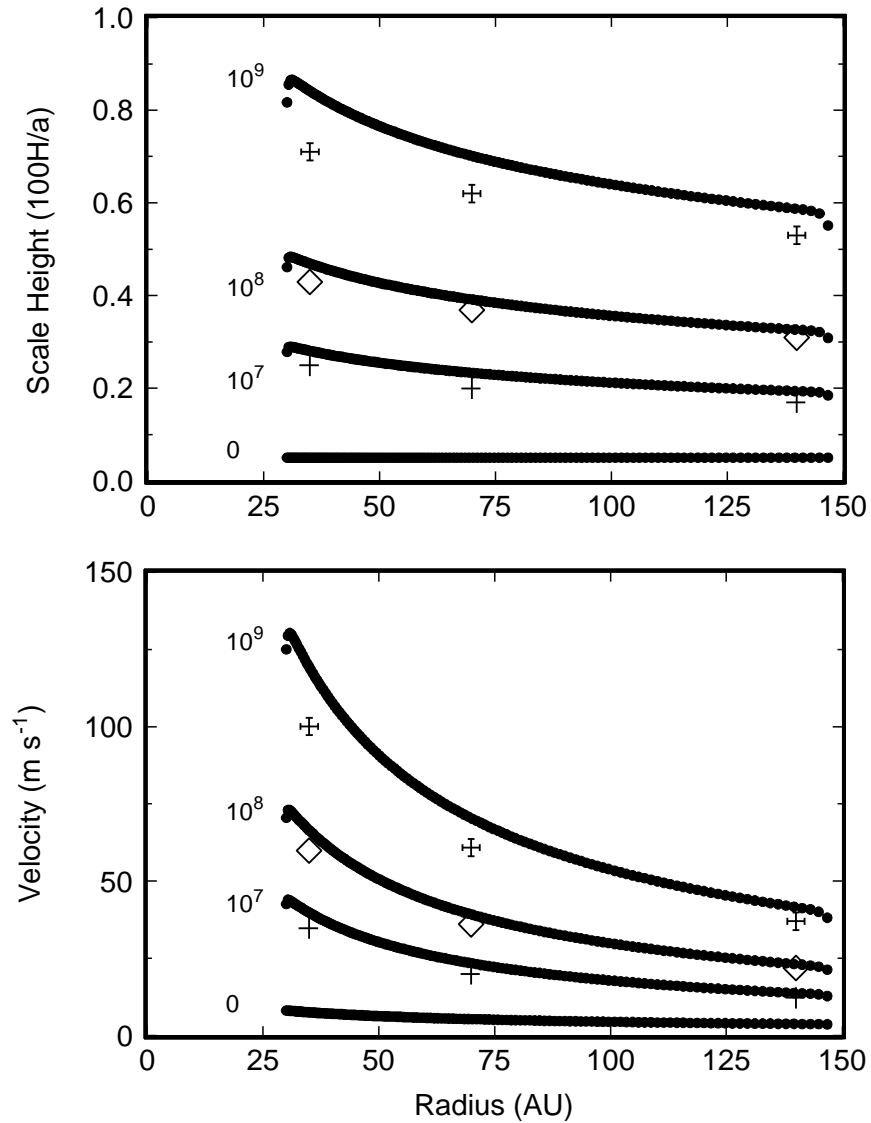


Fig. 4.— As in Figure 3, for 100 km planetesimals.

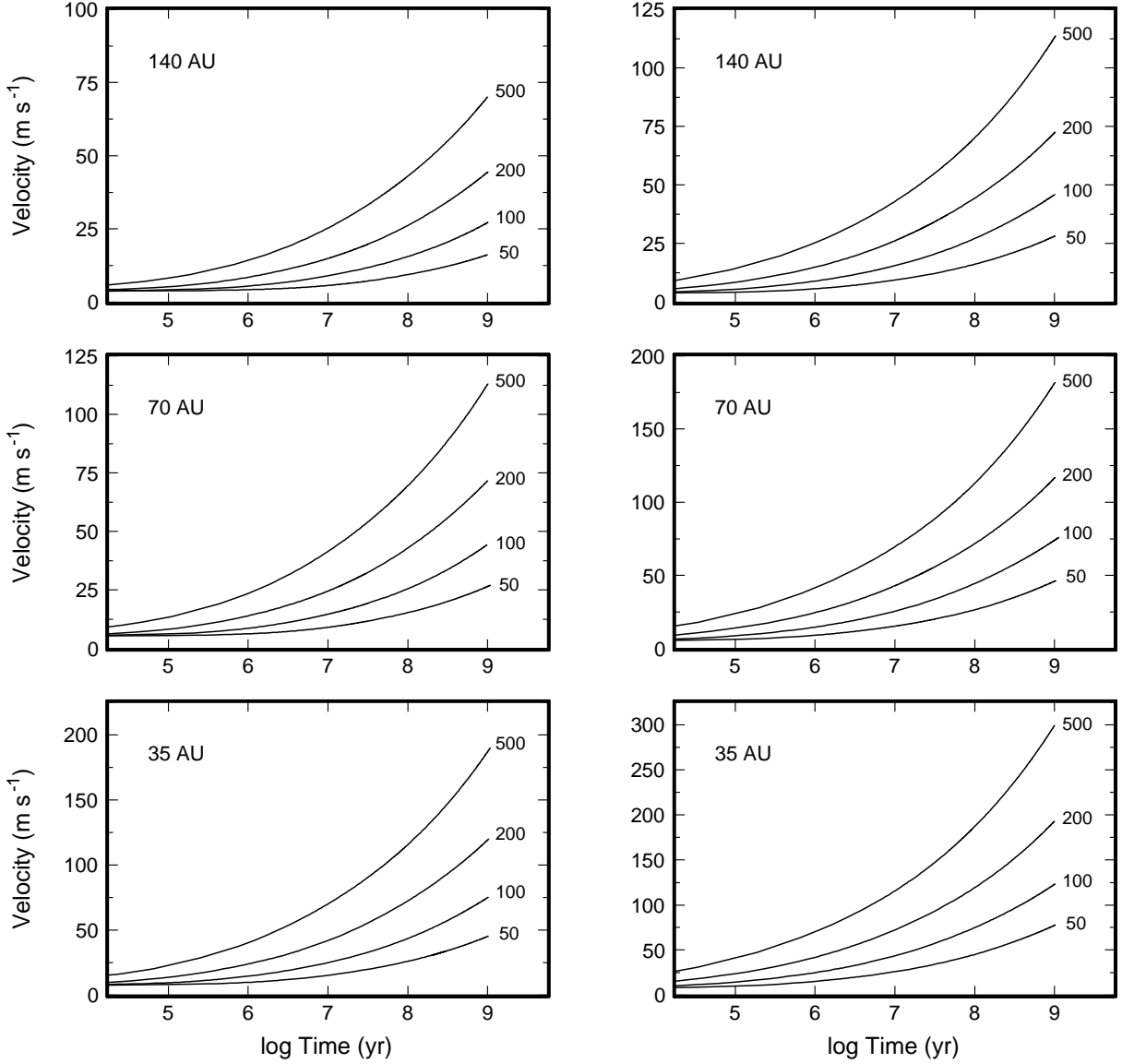


Fig. 5.— Evolution of particle velocity for a size distribution of planetesimals in orbit around a $3 M_{\odot}$ star at 35 AU (lower panels), 70 AU (middle panels), and 140 AU (top panels). The size distributions have equal mass per mass batch; the mass spacing factor is $\delta = 10^3$. The left panels show velocities for small planetesimals, with radii $\lesssim 1$ km, for disks with surface densities equivalent to the minimum mass solar nebula; the right panels show results for disks with 10 times the mass in a minimum mass solar nebula. The numbers to the right of each curve list the maximum size of the planetesimal in each calculation. Large planetesimals stir up disks more rapidly than small planetesimals.

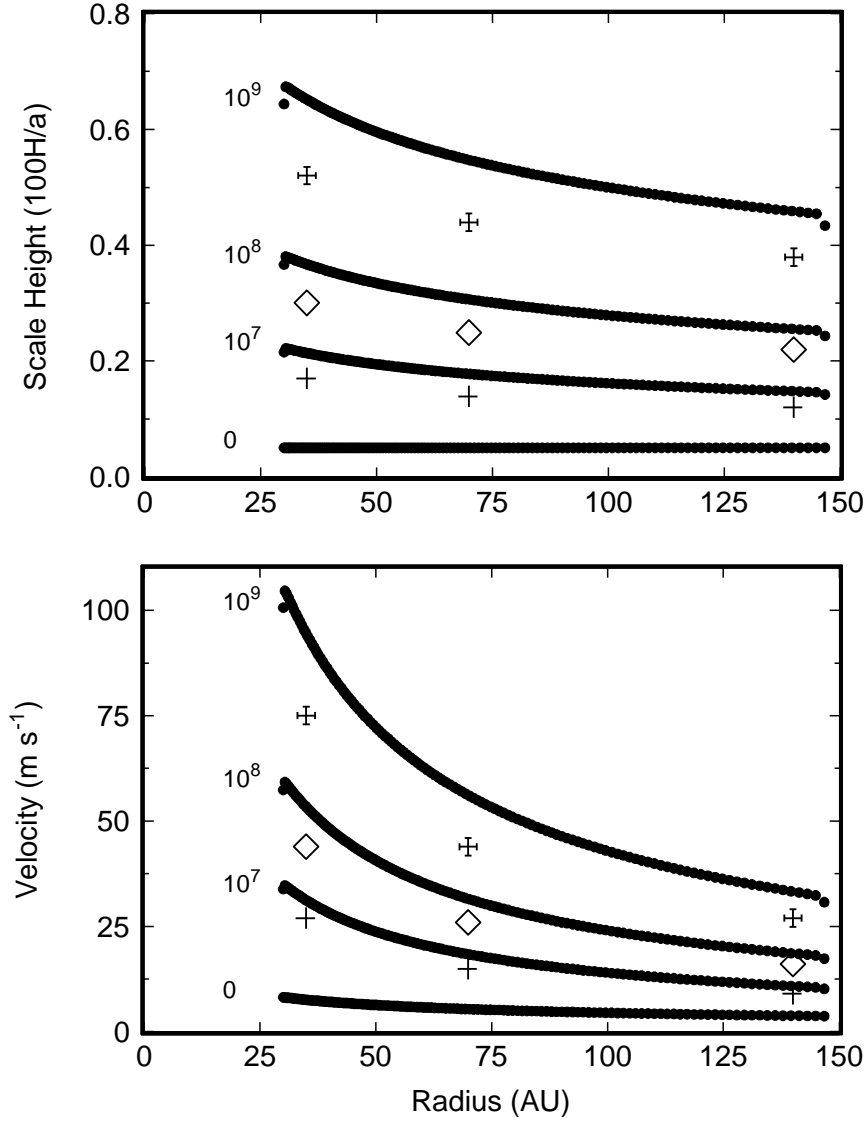


Fig. 6.— Evolution of particle velocity (lower panel) and vertical scale height (top panel) for small planetesimals of a size distribution of 1 m to 100 km planetesimals in a disk surrounding a $3 M_{\odot}$ star. The initial surface density in the disk is $\Sigma = 60(a/1 \text{ AU})^{-3/2}$. The evolution time in years is listed to the left of each curve.

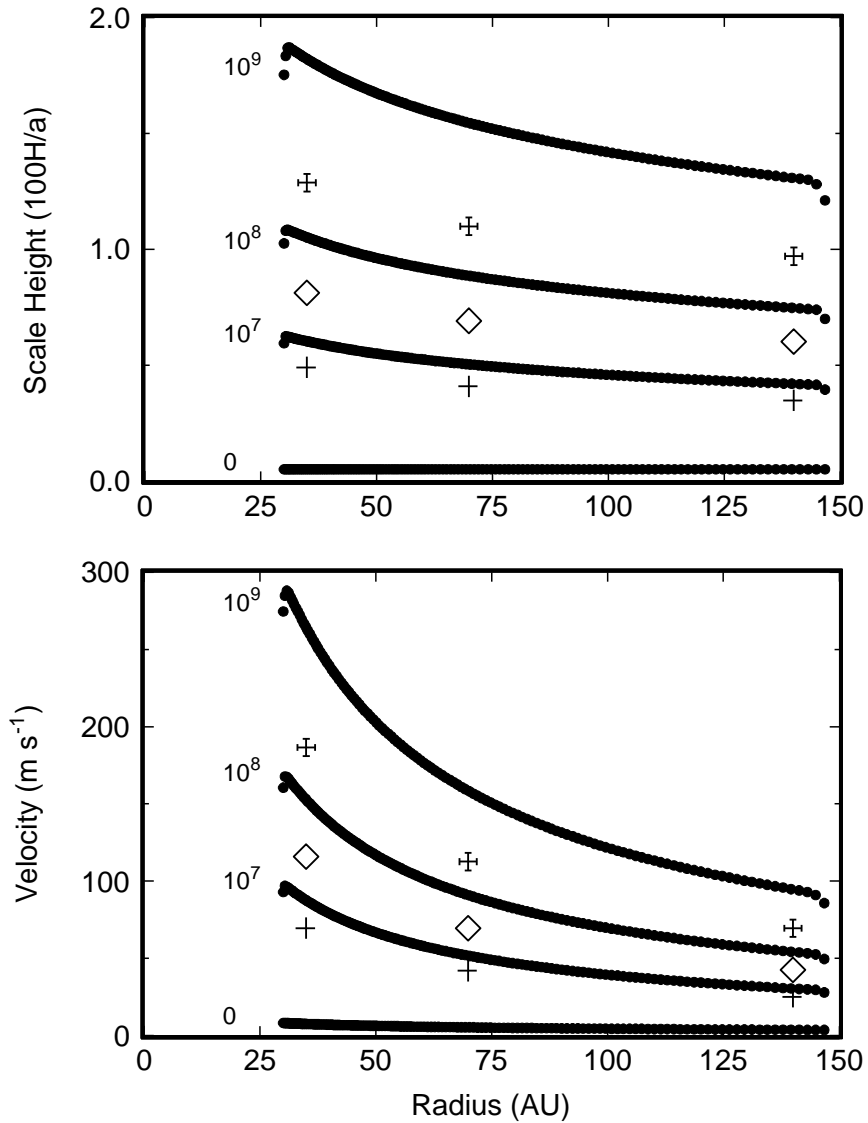


Fig. 7.— As in Figure 6, for a size distribution of 1 m to 500 km planetesimals.

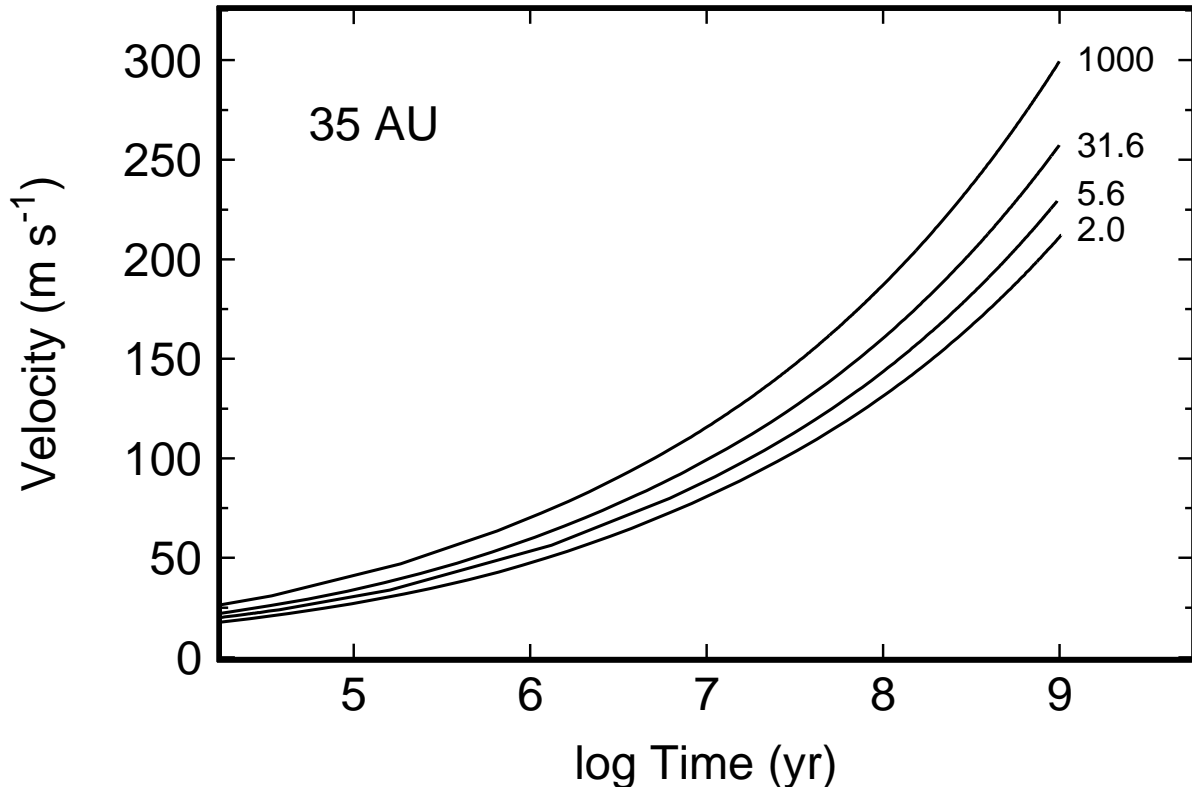


Fig. 8.— Evolution of particle velocity at 35 AU as a function of mass spacing factor, δ , indicated to the right of each curve. The curves show the variation of particle velocity for small planetesimals, with radii of 1 m to 1 km, in a size distribution with a maximum radius of 500 km and in a disk with surface density of 10 times the minimum mass solar nebula. Models with higher mass resolution achieve lower velocities compared to models with lower mass resolution.

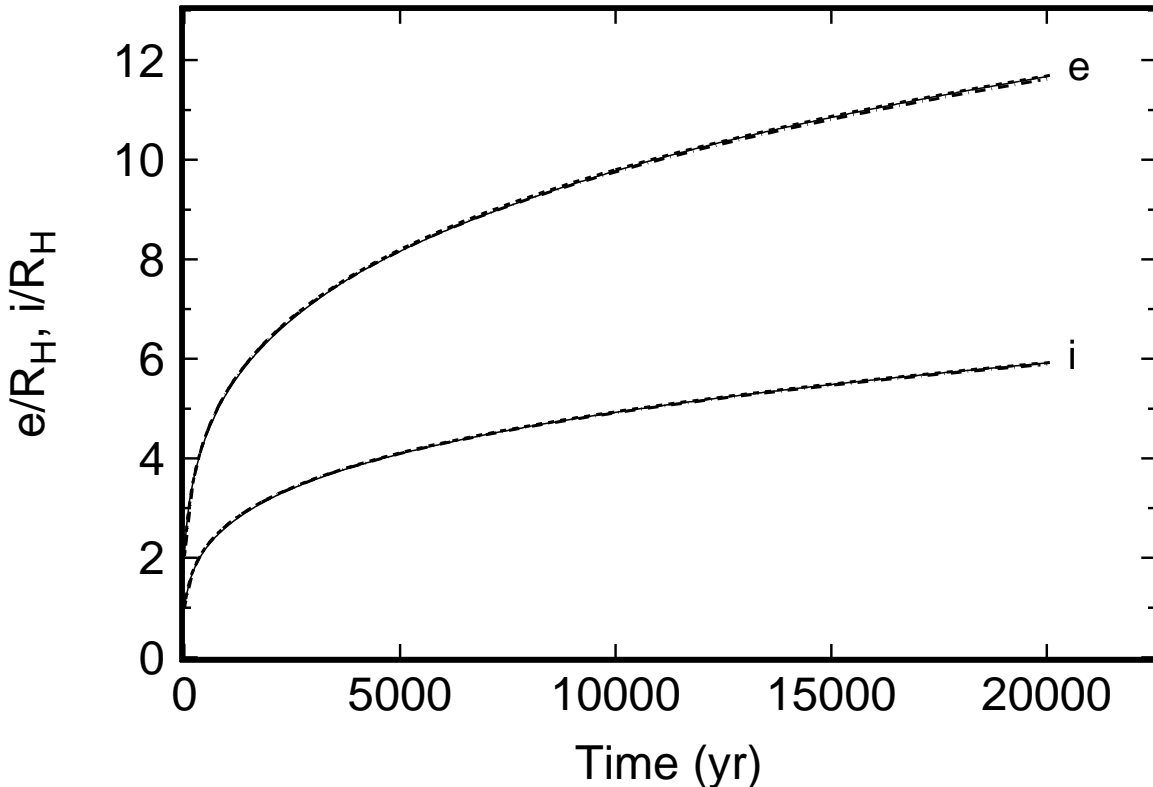


Fig. 9.— Evolution of e and i in units of the Hill radius for 800 planetesimals with $m_1 = 10^{24}$ g in grids with 20 (solid curves), 40 (dashed curves), and 80 (dot-dashed curves) annuli centered at 1 AU. The surface density for each grid is 10 g cm^{-2} at $t = 0$. The evolution of e and i is independent of the grid spacing.

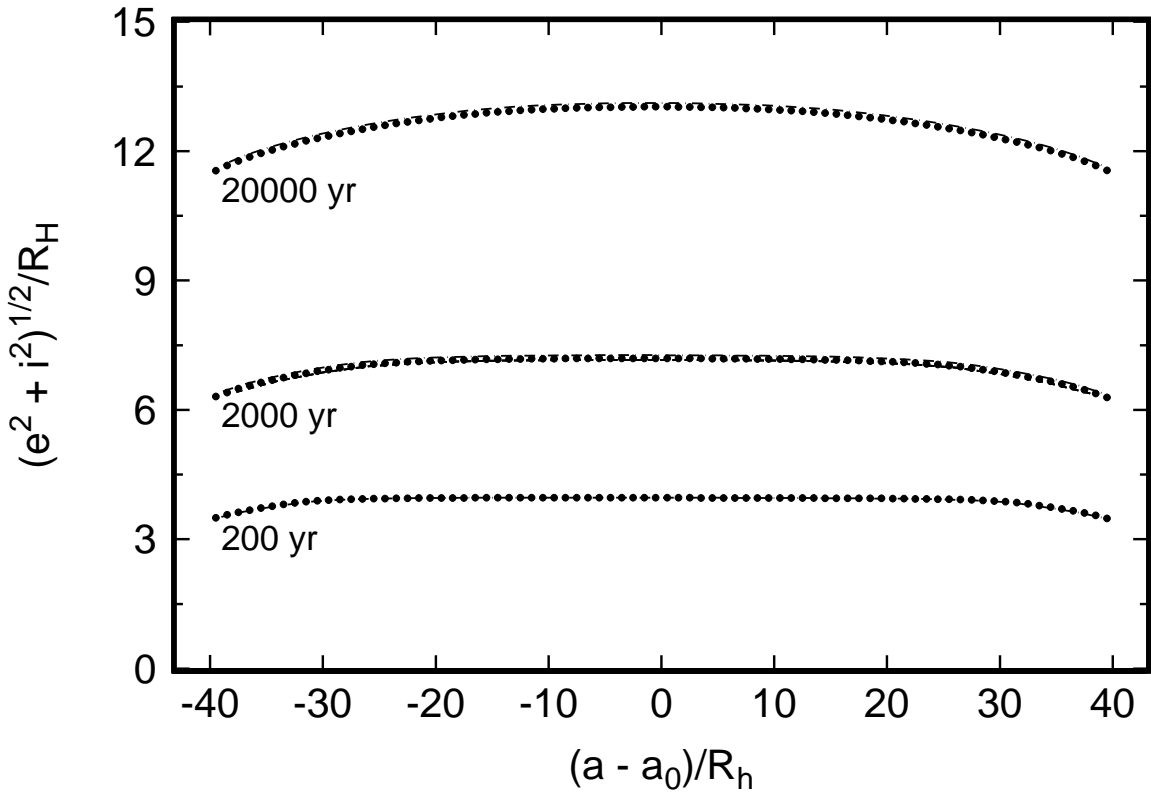


Fig. 10.— Evolution of the radial profile of $e^2 + i^2$ for the 800 planetesimal calculations in Figure 9. The filled symbols indicate $e^2 + i^2$ for a grid with 80 annuli. The curves plot results for a grid with 20 annuli (dashed curves) and for a grid with 40 annuli (dot-dashed curves). The evolution time is listed below each profile.

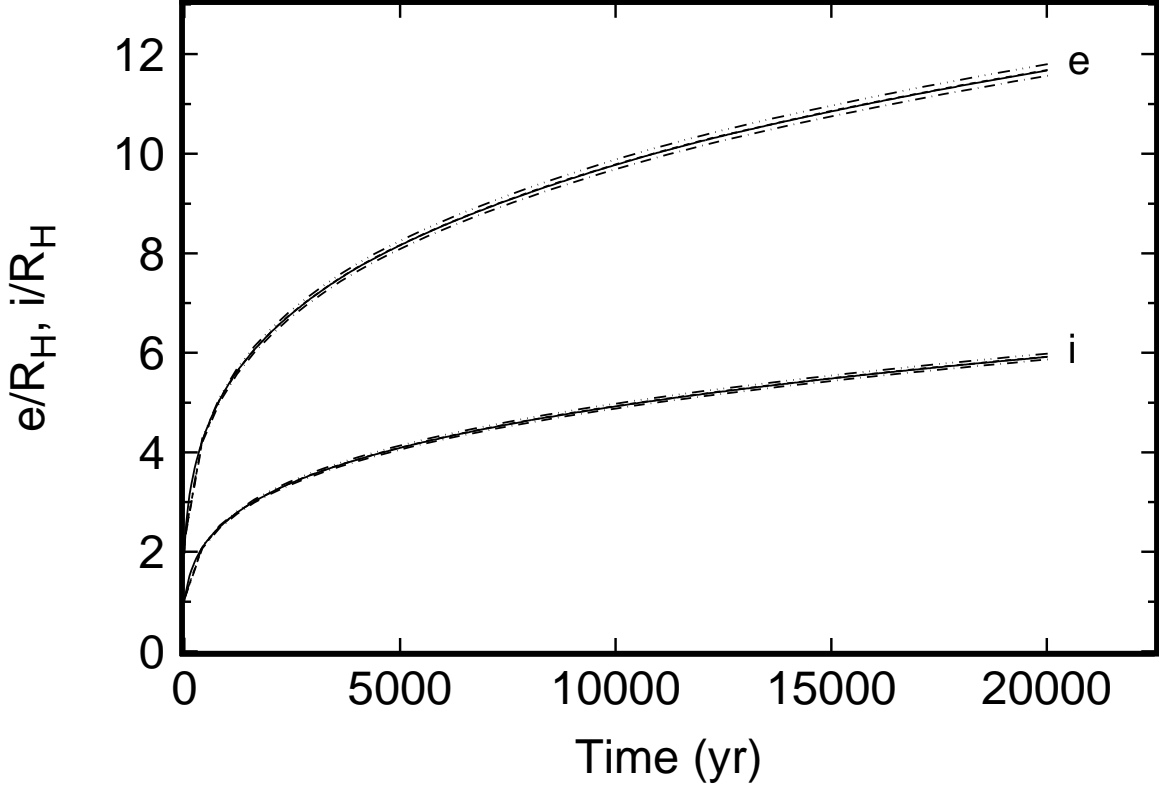


Fig. 11.— Scaled evolution of e and i in units of the Hill radius for planetesimals in a grid of 40 annuli centered at 1 AU. The four cases considered are 800 planetesimals with $m_1 = 10^{24}$ g (solid curves), 8000 planetesimals with $m_1 = 10^{24}$ g (dashed curves), 400 planetesimals with $m_1 = 10^{26}$ g (dot-dashed curves), and 4×10^5 planetesimals with $m_1 = 10^{23}$ g (dot-dot-dashed curves). The evolution time has been scaled with the surface density and planetesimal mass from equations (A14–A15).

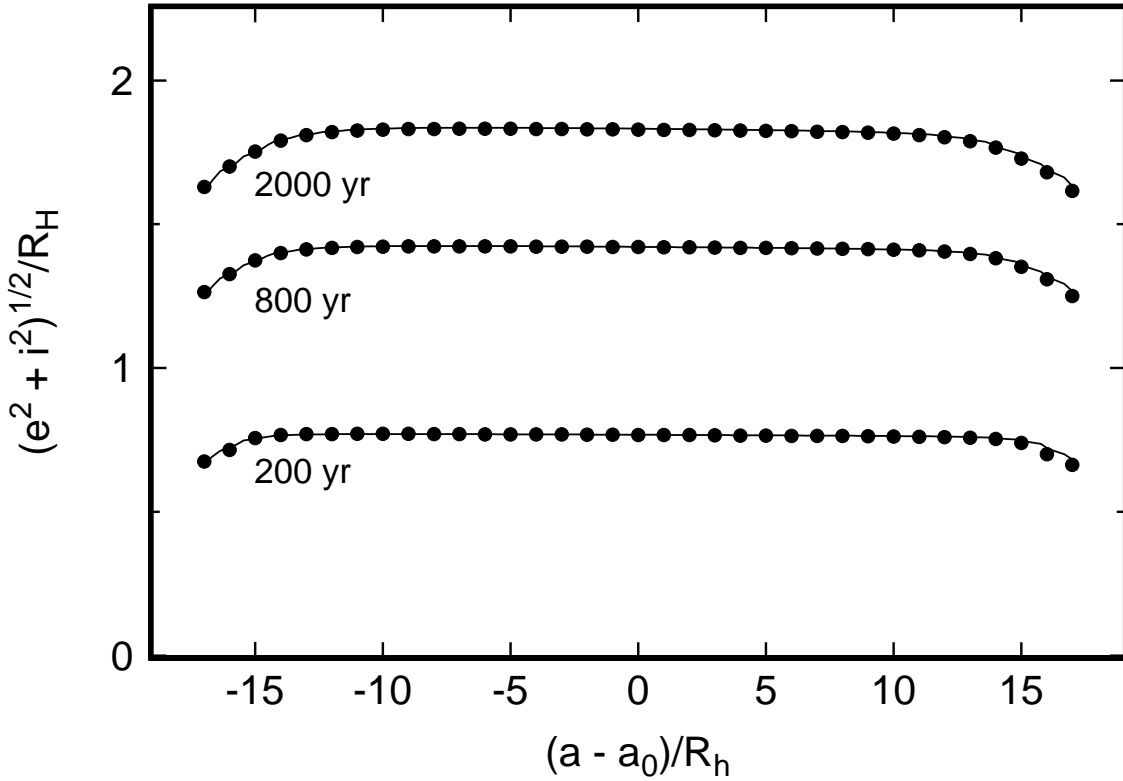


Fig. 12.— Evolution of the radial profile of $e^2 + i^2$ for 805 planetesimals in a grid centered at 1 AU. Filled circles indicate results for a grid of 35 annuli; the solid curve shows results for a grid of 70 annuli. Both grids extend to $\pm 17.5 R_H$ from the midpoint as described in the main text. The evolution time is listed below each profile.

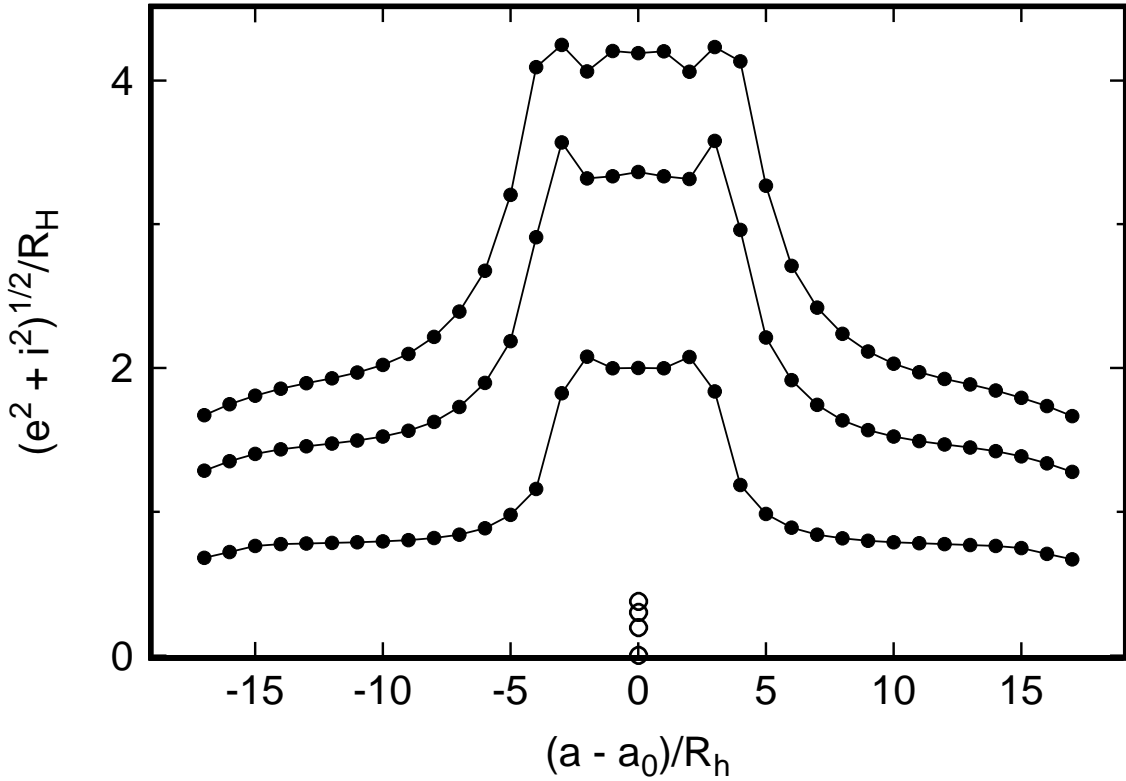


Fig. 13.— As in Figure 12, but with an additional planetesimal of mass $m_2 = 2 \times 10^{26}$ g at $a = a_0$. Open circles indicate the evolution of the massive planetesimal for $t = 0$ and other times as in Figure 12.

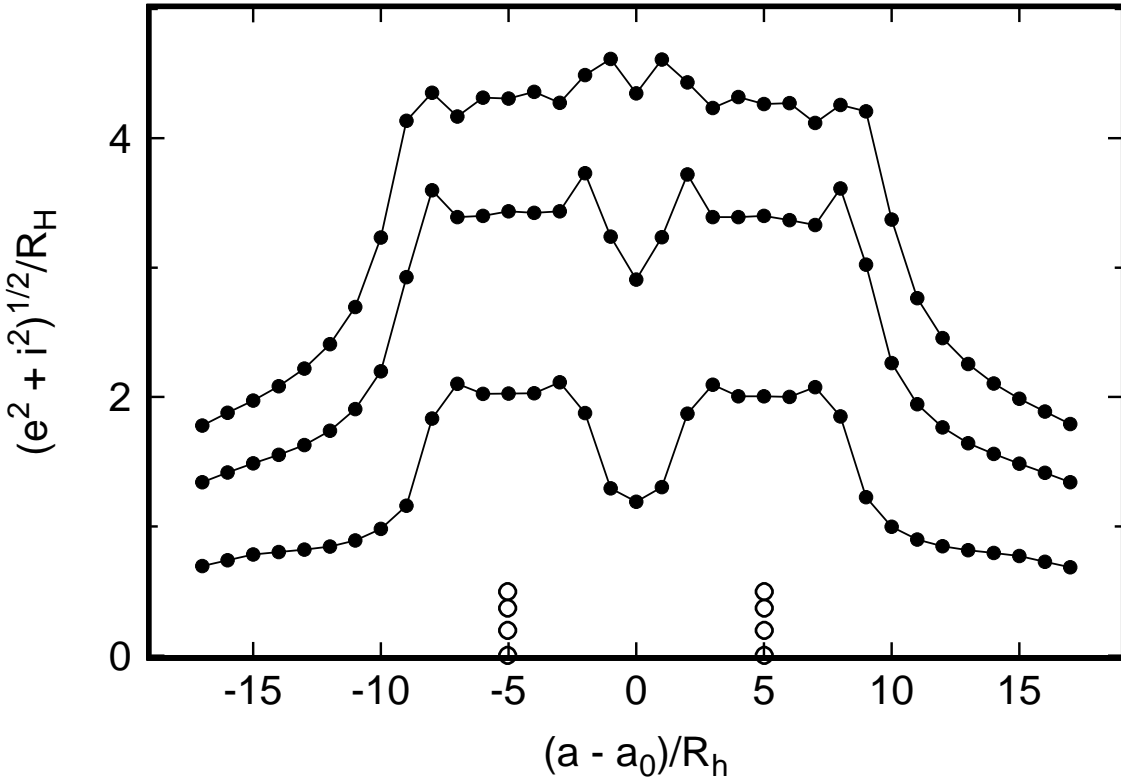


Fig. 14.— As in Figure 13, but with two planetesimals of mass $m_2 = 2 \times 10^{26}$ g at $a = \pm 5a_0$. Open circles indicate the evolution of the massive planetesimals for $t = 0$ and other times as in Figure 12.

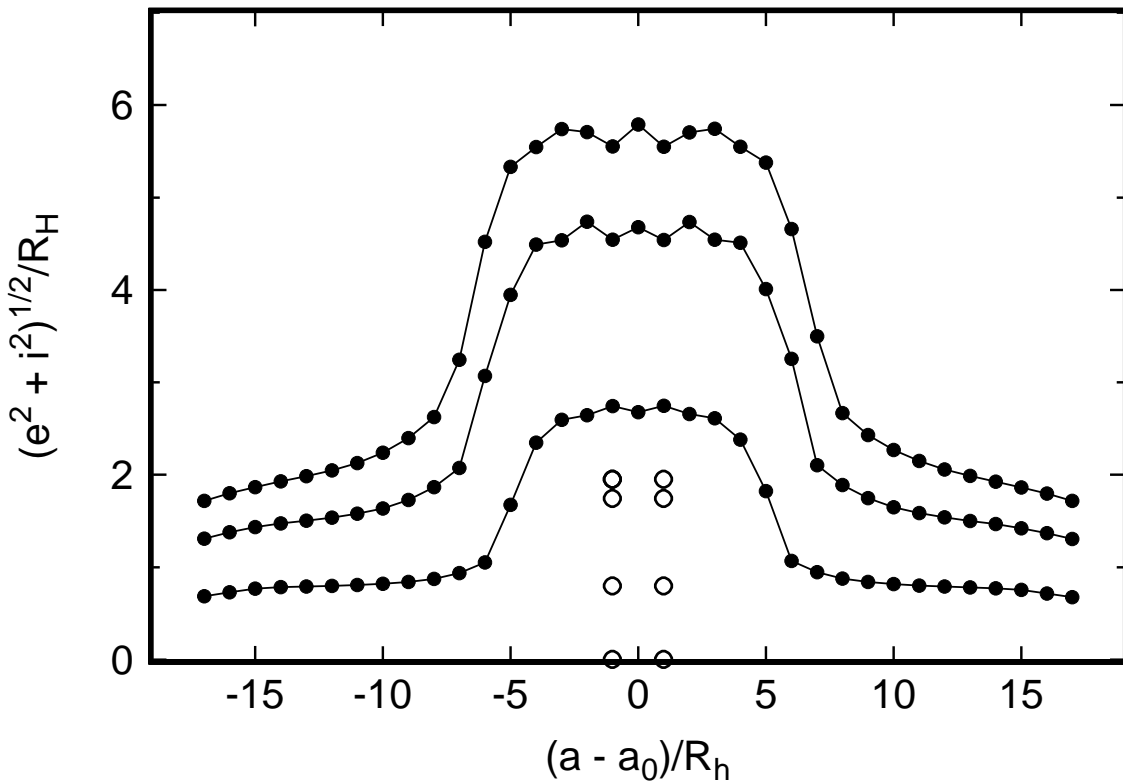


Fig. 15.— As in Figure 14, but with two planetesimals $a = \pm 2a_0$.

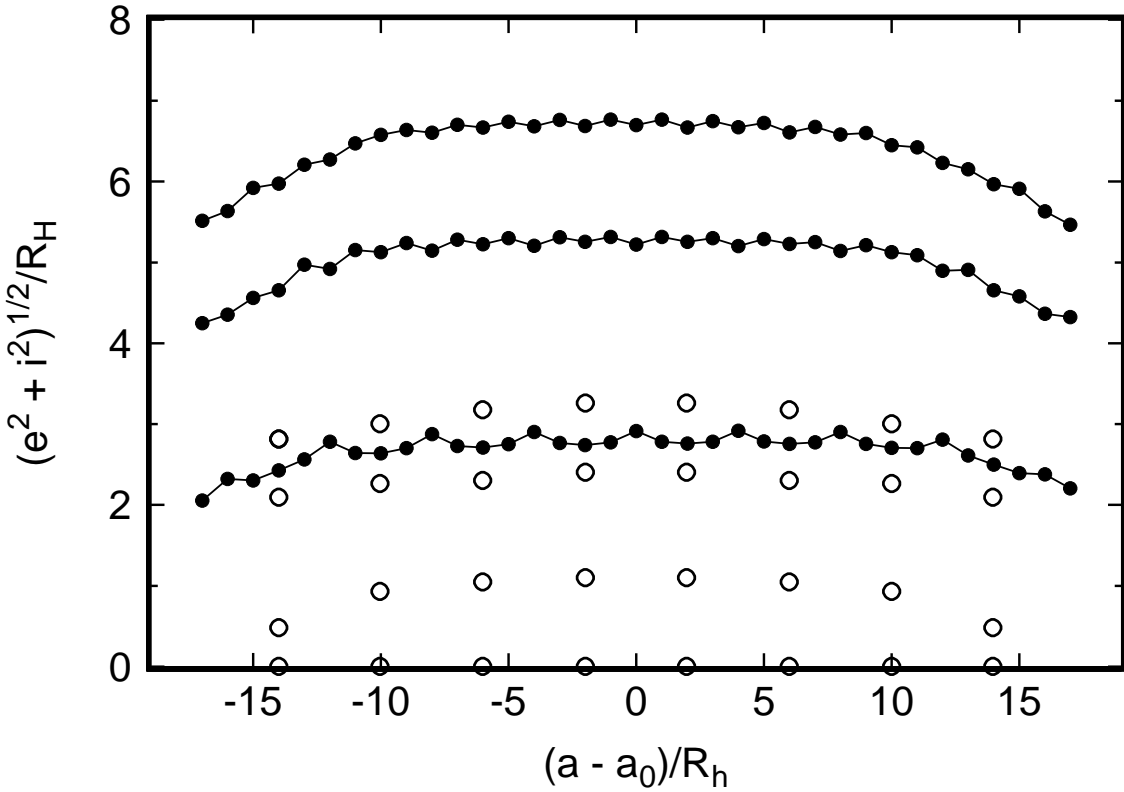


Fig. 16.— As in Figure 13, but with eight planetesimals of mass $m_2 = 2 \times 10^{26}$ g at $a = \pm 2a_0$, $\pm 6a_0$, $\pm 10a_0$, and $\pm 14a_0$.